A PDZ DOMAIN-CONTAINING PROTEIN IN MACROPHAGES

CHARACTERIZATION OF A PDZ DOMAIN-CONTAINING PROTEIN IN MACROPHAGES

By: EMMANUEL SAKARYA, B.Sc.

A Thesis Submitted to the School of Graduate Studies in Partial Fulfilment of the Requirements for the Degree Master of Science

MASTER OF SCIENCE (2021)	McMaster University, Hamilton, ON
TITLE:	Characterization of a PDZ domain-containing protein in macrophages
AUTHOR:	Emmanuel Sakarya, B.Sc. (Hons.) (McMaster University)
SUPERVISOR:	Bernardo L. Trigatti, B.Sc., Ph.D.
NUMBER OF PAGES:	xi, 95

ABSTRACT

Vulnerable atherosclerotic plaques are characterized by large necrotic cores and thin fibrous caps. Macrophage cell death is an important contributor to necrotic core size and high-density lipoprotein (HDL) has been shown to promote macrophage survival. Research has shown that HDL-dependent protection of macrophages is impaired in macrophages from *Pdzk1* knockout mice. However, little is known on the expression of *Pdzk1* in macrophages. In this study, we investigated *Pdzk1* expression in macrophages and its role in HDL-dependent protection of macrophages against necroptosis. Real-time quantitative reverse-transcriptase polymerase chain reaction and Western blotting were conducted on macrophages from wild type and two different *Pdzk1*-targeted mutant mice. We show that *Pdzk1* is expressed in macrophages. However, we also discovered that there is aberrant expression of truncated *Pdzk1* transcript(s) in macrophages from a commonly used *Pdzk1* global knockout mouse strain, although this was not the case in conditional *Pdzk1* knockout macrophages from a different mouse strain. Our findings indicate that the null mutation in macrophages from *Pdzk1* global knockout mice is not bona-fide and suggest for re-evaluation of the role of PDZK1 in HDL-signaling in macrophages. To investigate the role of PDZK1 in HDL-dependent protection of macrophages, we used conditional *Pdzk1* knockout macrophages and demonstrated that PDZK1 indeed promotes HDL-dependent protection against necroptotic cell death. This study confirms that *Pdzk1* is expressed in macrophages and clarifies its importance in HDL-dependent protection of macrophages from cell death.

ACKNOWLEDGEMENT

I sincerely thank my supervisor, Dr. Bernardo Trigatti, for entrusting me with a project that became the basis of my Master of Science thesis. I am grateful for his mentorship and guidance which honed my critical thinking skills. Our countless discussions have taught me the importance of using appropriate and calculated words when drawing conclusions and making scientific statements, which I know will remain a life lesson for me as I pursue my career. My graduate studies have been a memorable experience consisting of research and discovery and personal growth.

I also thank my supervisory committee members, Dr. Suleiman Igdoura and Dr. Ray Truant, for their constructive criticism and guidance during my committee meetings.

To the members of the Trigatti lab – thank you very much for your support and teachings, as well as the comradery and memories we developed over the past two years.

Finally, thank you to my family and friends for their continuous support and for entertaining discussions on my research; truly, PDZK1 has reached far more people than I would have expected. With relief, I conclude that macrophages do express PDZK1.

Table of Contents

LIST OF FIGURES

LIST OF ABBREVIATIONS

ANOVA	Analysis of variance
Apo	Apolipoprotein
ddH_2O	Double-distilled H_2O
CAD	Coronary artery disease
CVD	Cardiovascular disease
Csf1r	Colony-stimulating factor 1 receptor
DMEM	Dulbecco's Modified Eagle Medium
DMSO	Dimethyl sulfoxide
EDTA	Ethylenediaminetetraacetic acid
EGFP	Enhanced green fluorescent protein
FBS	Fetal bovine serum
HDL	High-density lipoprotein
HDL-C	High-density lipoprotein-cholesterol
HRP	Horseradish peroxidase
iCre	Inducible Cre
KO	Knockout
LDL	Low-density lipoprotein
Mer	Mutated mouse estrogen receptor
MLKL	Mixed-lineage kinase domain-like
NCLPDS	Newborn calf lipoprotein-deficient serum
NCS	Newborn calf serum

oxLDL	Oxidized low-density lipoprotein
PBS	Phosphate-buffered saline
PCR	Polymerase chain reaction
PDZ	Postsynaptic density-95/discs-large/zonula occludens-1
PDZK1	Postsynaptic density-95/discs-large/zonula occludens-1 domain containing 1
PI	Propidium iodide
PKA	Protein kinase A
PMA	Phorbol 12-myristate 13-acetate
PP	Primer-pair
PVDF	Polyvinylidene fluoride
qRT-PCR	Quantitative reverse-transcriptase polymerase chain reaction
RIPK	Receptor-interacting serine/threonine protein kinase
RT-PCR	Reverse-transcriptase polymerase chain reaction
SDS	Sodium dodecyl sulfate
SDS-PAGE	Sodium dodecyl sulfate polyacrylamide gel electrophoresis
SEM	Standard error of the mean
SR-B1	Scavenger receptor class B, type I
TAE	Tris-acetate-EDTA
TBS-T	Tris-buffered saline and Tween-20
TNF-α	Tumor necrosis factor-α
WT	Wild type

DECLARATION OF ACADEMIC ACHEIVEMENT

All work has been performed by Emmanuel Sakarya at the exception of the following:

- Figure 13: Yak Deng performed PCR and gel electrophoresis.
- Figure 14: Dr. George Kluck performed cell treatments and fluorescence imaging.

CHAPTER 1: INTRODUCTION

1.1.Cardiovascular Disease and Atherosclerosis

Cardiovascular disease (CVD), a disease of the heart and of the vasculature, is one of the leading causes of mortality globally[1]. In 2019, data from Statistics Canada identified CVD as the second leading cause of mortality behind malignant neoplasms[2]. Accordingly, CVD represents an enormous burden in healthcare expenditure[3]. CVD is an overarching term that constitutes numerous diseases such as coronary artery disease (CAD), cerebrovascular disease, and peripheral vascular disease[4]. The risk factors for developing CVD include hyperlipidemia, diabetes, hypertension, weight, smoking, alcohol, and a lack of exercise/sedentary lifestyle[5]. That said, atherosclerosis represents the major pathology that underlies most CVDs. Atherosclerosis is a chronic inflammatory disease of the arteries characterized by plaque buildup within arterial walls leading to the narrowing and hardening of the vessel[6]. Advanced atherosclerotic plaques are prone to rupturing, producing a thrombus which occludes blood flow to tissues, leading to a cardiovascular event such as myocardial infarction (heart attack).

1.2.Atherosclerosis Stages

Atherosclerosis initiation begins with endothelial activation and the accumulation of apolipoprotein (apo)-B-containing lipoproteins, mainly low-density lipoprotein (LDL), in the artery wall[6]. LDL is prone to accumulate in the walls at arterial branching points as well as the lesser curvature of vessels (i.e. the lesser curvature of the aortic arch) as blood flow is non-laminar in these regions[7]. LDL accumulation at these susceptible regions can become pathogenic. Specifically,

lipoproteins can undergo chemical modification (i.e. oxidation of LDL), which is a crucial step in atherogenesis as oxidized LDL (oxLDL) in turn activates the overlying endothelium. Moreover, the hemodynamics at these athero-prone regions creates irregular shear stress on the artery walls, thereby inducing endothelial activation/dysfunction[7]. Endothelial activation leads to chemokine secretion and up-regulation of adhesion molecules which promotes monocyte recruitment and extravasation[6]. Monocytes differentiate into macrophages as they enter the vessel wall (the intimal layer), engulfing native and modified LDL and in turn secreting chemokines to recruit additional leukocytes to the area. Eventually, macrophages become lipid-laden foam cells, which undergo apoptosis as a result of a combination of signals; endoplasmic reticulum stress due to accumulation of oxidized lipids and oxysterols amongst others, as well as extrinsic signaling, for instance via modified LDL and tumor necrosis factor-α (TNFα) recognized by pathogen recognition receptors and tumor necrosis factor receptor 1, respectively[8]. These apoptotic cells are cleared away by phagocytes in a process called efferocytosis[8]. As the disease progresses, efferocytosis fails and apoptotic cells accumulate. The underlying mechanism for this impairment is poorly defined but is believed to be multi-etiological. The inefficient clearing of apoptotic cells leads to secondary necrosis forming a necrotic core. Recent research has shown that lesional cells can also undergo necroptosis, a form of regulated necrosis, which contributes to the necrotic core[9]. Necroptosis occurs when caspase-8 is overwhelmed or inhibited as a result of synthetic (z-VAD-FMK) or endogenous (cIAPs) inhibitors. Caspase-8 inhibition prevents cellular apoptosis, allowing for receptor-

interacting serine/threonine protein kinase (RIPK)1 and RIPK3 to phosphorylate mixed-lineage kinase domain-like (MLKL), which oligomerizes and forms pores in the membrane causing lysis of the cell (Figure 1)[10]. Therefore, necroptosis releases cytoplasmic content, such as damage-associated molecular patterns, which increases the inflammatory burden of the lesion[11]. As the disease progresses, vascular smooth muscle cells from the medial layer of the vessel wall migrate into the intima in response to the inflammatory environment[12]. Some vascular smooth muscle cells adopt a phagocytic phenotype while others form a multi-cell layer below the endothelium, called a fibrous cap[12]. The fibrous cap is composed of secreted extracellular matrix, such as collagen, which strengthens and contains the plaque. As the plaque grows and the necrotic core enlarges, proteases originating from macrophages degrade the extracellular matrix[6]. Atherosclerotic lesions with large necrotic cores and thin fibrous caps are prone to rupturing, producing a thrombus that occludes blood flow and leads to a cardiovascular event.

1.3.High density lipoprotein (HDL) role in reverse cholesterol transport and cell signaling

HDL is commonly known as “good cholesterol” because of the association between high-density lipoprotein-cholesterol (HDL-C) and reduced risk of CVD[13]. Unlike LDL, HDL is not a substrate engulfed by macrophages driving foam cell formation. Instead, HDL is known to shuttle cholesterol and lipids from peripheral tissues, such as foam cell macrophages in the artery wall, to the liver (for secretion into bile or re-packaging into nascent lipoprotein particles) or to steroidogenic tissues (for steroid

hormone synthesis)[14,15]. This process of cholesterol shuttling is referred to as reverse cholesterol transport and is mediated by the high-affinity HDL receptor, scavenger receptor class B, type I (SR-B1, encoded by the *Scarb1* gene) which mediates the selective uptake of cholesteryl esters from HDL into hepatocytes and steroidogenic cells[14,16]. Accordingly, *Scarb1* knockout (KO) mice display increased plasma cholesterol found within abnormally large HDL particles[17]. In addition, PDZ domain containing 1 (*Pdzk1*[1]) KO mice display decreased hepatic SR-B1 protein levels and by consequence, increased serum HDL-C[18]. Restoration of PDZK1 in the livers of *Pdzk1* KO mice restores liver SR-B1 protein levels and consequently HDL-C[19]. Crossing these KO lines with atherosclerosis prone mouse strains (Apolipoprotein E (ApoE) KO and low-density lipoprotein receptor (LDLR) KO mice) leads to increased atherosclerosis [20–24].

Aside from reverse cholesterol transport, HDL has also been implicated in cellular signaling pathways[25]. Through its high-affinity receptor SR-B1, HDL promotes endothelial cell migration, survival and repair[25]. The intracellular signalling pathway, emanating from HDL-bound SR-B1 at the cell surface, involves the adaptor protein PDZK1, Src kinases, and phosphatidylinositol-3-kinase, which culminates in the activation of endothelial nitric oxide synthase, Akt kinase and Rac GTPase[25]. In addition, HDL has been implicated in cellular signaling in macrophages and cardiomyocytes, such as protection against cell death [24,26–28]. In macrophages, HDL has also been shown to

[1] *Pdzk1* refers to the mouse gene/mRNA, *PDZK1* refers to the human gene/mRNA, and PDZK1 refers to the mouse and human protein.

promote migration[29]. HDL-dependent protection of macrophages against cell death has been demonstrated to involve SR-B1 and PDZK1[24,26].

1.4.PDZK1

PDZ domain containing 1 (PDZK1) was originally discovered in human kidney epithelial cells[30]. It is expressed in a variety of cells and tissues, such as epithelial cells (kidney tubular cells, hepatocytes, intestinal mucosal cells) as well as in endothelial and myeloid cells[22,30,31]. Other aliases include Na+/H+ Exchange Regulatory Cofactor (NHERF3), C-terminal linking and modulating protein (CLAMP), CFTR-associated protein (CAP70)[32]. In both humans and mice, full-length *Pdzk1* transcripts are composed of a total of 9 exons. The canonical protein form is 519 amino acids (a.a.) in length with multiple isoforms in humans (four isoforms characterized as of yet) (NCBI; gene ID: 5174). No alternate isoforms have been reported in mice; all three mRNA transcript variants characterized code for the same 519 a.a. protein in mice (NCBI; gene ID: 59020). PDZK1 derives its name from its structure; it contains four PDZ protein-protein interaction domains[30]. A PDZ domain is composed of two alpha helices and six beta-strands; deriving its name from three proteins that contain such domains: postsynaptic density-95 (PSD-95), discs-large (Dlg), and zonula occludens-1 (ZO-1)[33,34]. PDZ domain-containing proteins bind preferentially (but not exclusively) to the carboxy-terminus of their targets[33–35]. PDZ-containing proteins often have multiple PDZ domains thereby acting as scaffolds – bridging/clustering proteins to influence cellular functions[36,37]. PDZK1 has four of these domains and interacts with many proteins. Most of the proteins PDZK1 has been shown to bind are ion transporters (Na^+/H^+ exchangers,

cystic fibrosis transmembrane regulator, Na^+-P_i cotransporters, urate-anion exchanger 1, ATP-binding cassette transporter protein C2, among others)[38–41]. However, it also interacts with the HDL receptor scavenger receptor class B, type I (SR-B1)[42] and is reported to play a role in atherosclerosis.

Extensive studies on *Pdzk1* KO mice show that PDZK1 protein is required for SR-B1 protein stabilization in the liver and intestine but not in steroidogenic tissues (adrenal, ovary and testis), endothelial cells, or macrophages[18,22]. Moreover, SR-B1 protein stabilization in the liver depended on PDZK1 binding to SR-B1, which involved the QEAKL peptide sequence on the carboxyl-terminus of SR-B1. The QEAKL segment binds (through hydrogen bonds and hydrophobic interactions) to PDZ domain 1 (high affinity interaction) and PDZ domain 3 (low affinity interaction) of PDZK1[43,44]. Hepatic SR-B1 protein expression, localization and function requires PDZ domain 1 and 4, which bind to SR-B1 and membrane lipids, respectively[45]. PDZ domain 3 plays a redundant role in binding to SR-B1 and the function of PDZ domain 2 is unrelated to SR-B1 (neither domain function as spacers)[45]. Moreover, the carboxy-terminus of PDZK1 contains the protein kinase A (PKA) phosphorylation motif RXXS which, when phosphorylated, increases stabilization of SR-B1 protein in rat liver[46]. This phosphorylation motif is also conserved in mouse and human PDZK1. As described above, *Pdzk1* KO mice display decreased hepatic SR-B1 protein levels and increased serum HDL-C[18], and the correction of this phenotype requires PDZ domains 1-4 of PDZK1 but not its phosphorylation motif, suggesting that the phosphorylation motif is not required for steady-state expression/function of hepatic SR-B1 but is required for its regulation[19]. In addition to

lipid metabolism, PDZK1 is involved in cellular signaling in macrophages. Although PDZK1 does not stabilize SR-B1 protein in macrophages, it is believed to bind to SR-B1 in macrophages and participate in HDL cell signaling. PDZK1 has been shown to promote HDL-survival (protection against apoptosis and necroptosis) and migration, and HDL-independent efferocytosis [24,29,47].

1.5. Macrophage Survival (HDL-dependent protection against apoptosis) and PDZK1

Apoptosis is the most common form of regulated cell death and can be activated via intrinsic or extrinsic pathways (Figure 1 displays the extrinsic pathway induced by TNF-α)[48]. Both pathways lead to the activation of cysteine-dependant aspartate proteases (caspases) which carry out cell death by degrading proteins and promoting cell corpse clearance[49]. The plasma membrane of the dying cell begins to bleb, forming smaller apoptotic bodies. Apoptotic cells and bodies display "eat-me" signals on their membranes allowing their clearance by phagocytes. This process is anti-inflammatory and "immunologically silent" as the pro-inflammatory content within apoptotic cells is not released. Moreover, the engulfment of apoptotic bodies activates anti-inflammatory pathways within phagocytes, ultimately maintaining an immunologically silent environment[50].

Macrophage apoptosis plays a dichotomous role in atherosclerotic progression based on the stage of the disease.[51] In early-stage plaques, apoptosis is favorable because efferocytosis is effective. Apoptotic cells can efficiently be cleared away by phagocytes thus reducing lesion cellularity and lesion growth[51]. In advanced plaques, apoptosis is

unfavorable as efferocytosis is defective. Thus, apoptotic cells are not cleared away promptly leading to secondary necrosis. This increases inflammation and necrotic core size, ultimately de-stabilizing the plaque.[8,51]

High density lipoprotein (HDL) was shown to promote Akt phosphorylation and survival in endothelial cells and macrophages[24,26,52]. This anti-apoptotic signaling in macrophages appears to be mediated by SR-B1 (unpublished work from our laboratory) and shown to require PDZK1[24,26]. *In vitro* studies from our laboratory demonstrated that macrophages from *Pdzk1* KO mice displayed blunted HDL-dependent activation of Akt and blunted HDL-dependent survival of macrophages when challenged with different apoptotic stimuli (oxLDL, ultraviolet radiation, tunicamycin), as indicated by terminal deoxynucleotidyl transferase nick end labeling (TUNEL) staining[24,26]. Moreover, *in vivo* work has shown that *Ldlr* KO mice transplanted with bone marrow from *Pdzk1* KO mice displayed increased apoptotic cells in atherosclerotic plaques and increased necrotic core size compared to control *Ldlr* KO mice with wild type bone marrow, when fed a high-fat diet[24]. These results suggest that *Pdzkl* expressed in macrophages likely plays an athero-protective role.

1.6.Macrophage Survival (HDL-dependent protection against necroptosis) and PDZK1

Necroptosis is another form of regulated cell death that is caspase-independent and pro- inflammatory. This pathway is mediated by receptor-interacting serine/threonine-protein kinase 1 and 3 (RIPK1 and RIPK3) and mixed-lineage kinase domain-like (MLKL) proteins (Figure 1)[48]. It is essential that pro-apoptotic caspase-8 is

inhibited (or overwhelmed) for necroptosis to occur, otherwise caspase-8 will cleave RIPK1 and RIPK3 and induce apoptosis instead. Necroptosis can be stimulated by extrinsic and intrinsic pathways[48]. These pathways lead to phosphorylation of MLKL by RIPK1 and RIPK3, in which phospho-MLKL oligomerizes, translocates to the plasma membrane, forms pores and disrupts membrane integrity, ultimately releasing intracellular content (Figure 1). Hence, necroptosis is pro-inflammatory and immunogenic. In addition to apoptosis, necroptosis has recently been implicated in atherosclerosis[9,53,54]. The induction of necroptosis (as well as apoptosis) is stimulated through overlapping receptors and signal transduction pathways, such as via toll-like receptors, tumor necrosis factor receptor 1, pathogen recognition receptors, and the FAS receptor.[48]

Extensive work from our laboratory has shown that PDZK1 is involved in HDL-dependent protection of macrophages against necroptosis (manuscript under review). Necroptosis can be induced experimentally by treating cells with a cell death inducer (e.g. oxidized LDL or TNF-α) and the synthetic pan-caspase inhibitor z-VAD-FMK (to inhibit apoptosis). Necroptotic cell death can be visualized using vital nuclear stains which are excluded from intact, healthy cells but can enter via the compromised membranes of necrotic cells and stain nuclear DNA. Our laboratory has shown that HDL protects macrophages from oxLDL + z-VAD-FMK or TNF-α + z-VAD-FMK-induced necroptosis but this protection was impaired in macrophages from *Pdzk1* KO mice. This protection was also shown to require Akt and PI3K, similar to the mechanism for HDL-dependent protection of macrophages from apoptosis.

Despite our laboratory's findings demonstrating that PDZK1 is involved in macrophage function by promoting HDL-dependent survival[24,29], others have reported that mouse peritoneal macrophages and human THP-1 macrophages do not express *Pdzk1* mRNA (without providing supporting data)[47,55]. This is in disagreement with our laboratory's findings that have shown a phenotype associated with macrophages from *Pdzk1* KO mice. There is therefore a need to re-examine *Pdzk1* expression in macrophages and clarify how the *Pdzk1*-targeting mutation used to create the *Pdzk1* KO mice influences HDL-signaling in macrophages.

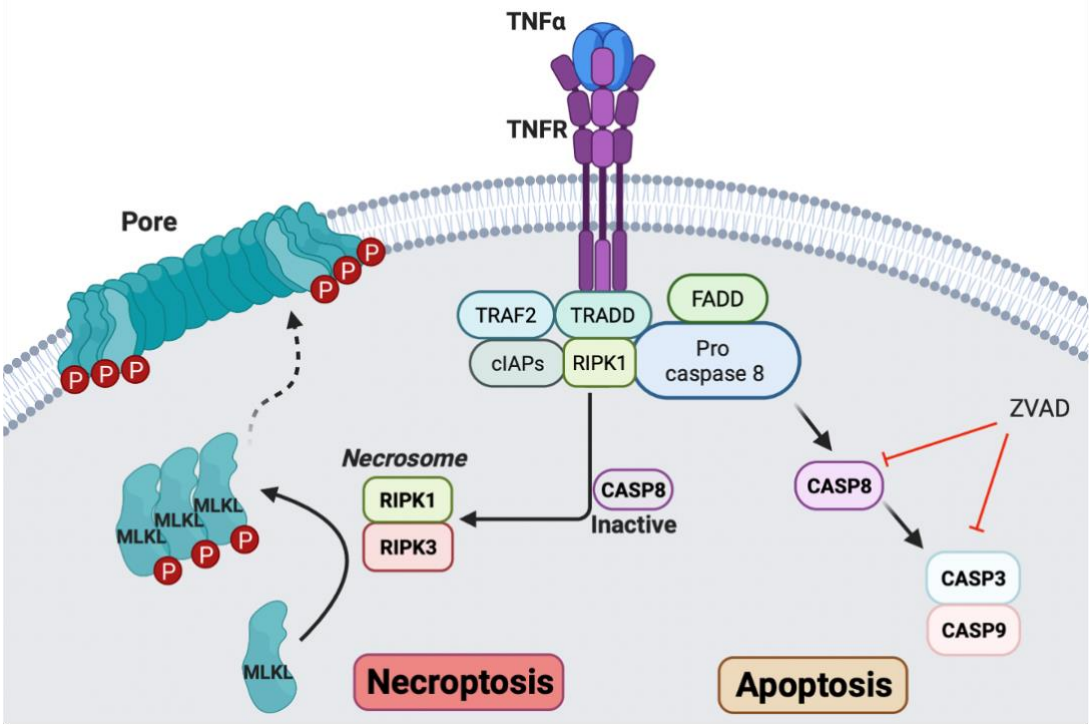

Figure 1: Extrinsic cell death signaling pathway: crossroads between necroptosis and apoptosis.

TNF-α binds to its cognate receptor tumor necrosis factor receptor (TNFR) on the cell membrane, promoting the recruitment and activation of cell death proteins such as RIPK1, RIPK3, and pro-caspase-8. Activated caspase-8 promotes apoptosis by activating caspase-3 and caspase-9. Caspase-8 inhibits necroptosis by cleaving RIPK1 and RIPK3. However, if caspase-8 is inactive (inhibited experimentally by a synthetic molecule, z-VAD-FMK, or biologically by cIAPs), the cell undergoes necroptosis. During necroptosis, RIPK1 and RIPK3 oligomerize into an amyloid structure called the necrosome, which phosphorylates MLKL. Phospho-MLKL oligomerizes in the cytoplasm and translocates to the plasma membrane where it will form pores, leading to lysis of the cell and release of cytoplasmic content such as damage-associated molecular patterns.

CHAPTER 2: HYPOTHESIS AND OBJECTIVES

2.1 Aim

Our laboratory has reported that *Pdzk1* KO in mouse macrophages impacts efferocytosis and HDL-dependent survival and migration [24,29]. However, others have suggested that *Pdzk1* is not expressed in macrophages [47,55]. Therefore, the aims of this study are to re-examine *Pdzk1* expression in macrophages and to understand the mechanism(s) by which KO of *Pdzk1* impacts macrophage responses to HDL.

2.2 Hypothesis

We hypothesize that macrophages express *Pdzk1* and that *Pdzk1* gene disruption resulting in a lack of *Pdzk1* expression in macrophages would impair HDL-dependent protection of macrophages from necroptotic cell death.

2.3 Objectives

1. Determine if mouse and human macrophages express *Pdzk1*.
2. Assess how a *Pdzk1*-targeting mutation in mice (*Pdzk1* global KO mice available from The Jackson laboratory[56]) affects *Pdzk1* expression in macrophages.
3. Assess how a conditional *Pdzk1*-targeting mutation in mice affects *Pdzk1* expression in macrophages[57].
4. Determine if the conditional *Pdzk1*-targeting mutation in macrophages influences HDL-dependent protection against necroptosis.

CHAPTER 3: METHODS AND MATERIALS

3.1. Mice

All procedures conducted on mice were approved by McMaster University's Animal Research Ethics Board and performed in accordance with the Canadian Council on Animal Care guidelines. Mouse strains used were C57BL/6J (obtained from The Jackson Laboratory; stock No. 000664), *Pdzk1-/-* (on a B6129SF2/J background; obtained from The Jackson Laboratory (Bar Harbor, ME, USA); stock No. 006208), and *Csf1r-iCre Pdzk1*$^{flox/flox}$ *ROSA26*$^{mT/mG}$ mice (see section below for mouse information, breeding, and tamoxifen injections). Mice were bred and housed in the David Braley Research Institute (DBRI) animal facility in ventilated cages with automatic watering and free access to food (standard chow diet). Mouse strains used are indicated in the figure captions of each experiment.

3.2. *Csf1r-iCre Pdzk1*$^{flox/flox}$ *ROSA26*$^{mT/mG}$ mice and Tamoxifen injections

The *Csf1r-iCre Pdzk1*$^{flox/flox}$ *ROSA26*$^{mT/mG}$ mouse strain was developed by the laboratory technician, Yak Deng, using the following three mouse strains. Mice expressing tamoxifen-inducible Mer-iCre-Mer fusion protein under the control of macrophage-specific mouse *Csf1r* promoter (Stock No. 019098; *FVB-Tg(Csf1r-cre/Esr1*)* were purchased from The Jackson Laboratory (Bar Harbor, ME). *Pdzk1*$^{flox/flox}$ *ApoE-/-* mice [57] were kindly provided by Dr. Phil Shaul and Dr. Chieko Mineo groups (University of Texas Southwestern Medical Center, Dallas, TX) and were outbred to mice bearing wild type *ApoE* to put the *Pdzk1*$^{flox/flox}$ mutation on an *ApoE* wild type background. ROSA26$^{mT/mG}$ mice (Stock No. 007676, B6.129(Cg*)-Gt(ROSA)26Sor*$^{tm4(ACTB-}$

tdTomato,-EGFP)Luo) were purchased from The Jackson Laboratory and express the membrane-targeted TdTomato red-fluorescent protein (encoded by the *mT* gene). In cells expressing iCre, *mT* is deleted and expression of the downstream *mG* gene occurs producing the membrane-targeted enhanced green fluorescent protein (EGFP).

Csf1r-iCre Pdzk1$^{flox/flox}$ *ROSA26*$^{mT/mG}$ mice were injected intra-peritoneally with 166 mg tamoxifen/kg mouse/day for five consecutive days. The following 2mL solution (adequate to inject four mice weighing 30g) was prepared; 0.1g tamoxifen (Sigma-Aldrich; cat: T5648) was dissolved in 200µL of 100% ethanol and vortexed for ~1 min. The volume was adjusted to 2mL with corn oil (Sigma Aldrich; cat: C8267), producing a final concentration of 0.05 g/ml (50 mg/mL) of tamoxifen, and vortexed for another ~1 min. A control (vehicle) solution was prepared by following the same steps but excluding tamoxifen. Tamoxifen and vehicle solutions were protected from light by wrapping the tubes in aluminum. Solutions were incubated at 37°C, on a rotator in the hot room, overnight. The following day, mice were anesthetized with isoflurane (flow vaporizer set to 5%) supplied with oxygen (flow rate: 1 L/min) and were injected intra-peritoneally with 100µL of vehicle or 100µL of tamoxifen (to administer 5 mg of tamoxifen for a 30g mouse). Cre-positive and Cre-negative *Pdzk1*$^{flox/flox}$ *ROSA26*$^{mT/mG}$ mice were injected with either tamoxifen or vehicle producing 4 different treatment groups. Injections were performed for five consecutive days (tamoxifen and vehicle solutions were stored at 4°C until the following day when they were placed on the rotator at 37°C for at least an hour, prior to injecting mice). Peritoneal macrophages were harvested one week following the

last injection, therefore mice were injected with 1mL of 10% thioglycollate four days prior to the harvesting date to induce peritonitis.

3.3. Cell culture

All cells were cultured in a humidified incubator set to 37°C with 5% CO_2. Peritoneal macrophages were obtained from mice by intra-peritoneal injection of 1 mL 10% thioglycollate to recruit macrophages to the peritoneum. Four days later, mice were euthanized by CO_2 administration. Peritoneal macrophages were harvested by peritoneal lavage using 10 mL of ethylenediaminetetraacetic acid (EDTA) (5mM) in phosphate-buffered saline (PBS)(137mM NaCl, 2.7mM KCl, 10mM Na_2HPO_4, 1.8mM KH_2PO_4, pH 7.4). Following peritoneal lavage, a piece of the large lobe of the liver was isolated and flash frozen in liquid nitrogen for subsequent analysis by sodium dodecyl sulfate polyacrylamide gel electrophoresis (SDS-PAGE) and Western blotting. Macrophages were centrifuged and washed with warmed Dulbecco's Modified Eagle Medium (DMEM) (Multicell; cat: 319-015) to remove EDTA and re-suspended in DMEM supplemented with 10% fetal bovine serum (FBS) (Wisent Bioproducts; cat: 080-150), 2 mM L-glutamine, 50 µg/mL penicillin and 50 U/mL streptomycin (Wisent Bioproducts; cat: 450-201) (peritoneal macrophage complete growth medium). For fluorescence experiments, peritoneal macrophages were seeded at 1.5 x 10^5 cells per well (0.8cm^2) of an 8 well-chamber slide (BioBasic; SP41219). 2 hours following seeding of macrophages, media was aspirated to remove non-adherent fibroblasts and red blood cells, and then complete medium was added back. Cells were cultured overnight. The next day, media was changed to DMEM + 3% newborn calf lipoprotein-

deficient serum (NCLPDS; prepared as previously described [58]) for 24h (to starve the cells of lipoproteins) and then treated as per the HDL-dependent protection against necroptosis experiment described below.

THP-1 monocytes were cultured in Roswell Park Memorial Institute (RPMI)-164 medium (Wisent Bioproducts; cat: 350-000) supplemented with 10% FBS, 2 mM L-glutamine, 50 µg/mL penicillin and 50 U/mL streptomycin (THP-1 monocyte complete growth medium). Cells were grown in T-75 flasks and sub-cultured every 3-4 days as follows; cells were counted and plated in T-75 flasks at a concentration of 1 x 10^6 cells/mL in 20mL of complete media. THP-1 monocytes were differentiated to macrophages by adding phorbol 12-myristate 13-acetate (PMA) to the media at a final concentration of 100 ng/mL. Cells were allowed to differentiate for 48h.

3.4. SDS-PAGE and immunoblotting

Cells were lysed with 1X radioimmunoprecipitation (RIPA) buffer (50 mM Tris-HCl at pH 7.4 containing 150 mM NaCl, 1% Triton X-100, 1% sodium deoxycholate, 0.1% SDS and 1 mM EDTA) supplemented with proteinase inhibitors: pepstatin A (1 µg/mL), 4-amidinophenyl methanesulfonyl fluoride (50 µM), aprotinin (10 µg/mL), leupeptin (1 µg/mL). Liver samples were homogenized using an Ultra-Turax T8 (IKA Labortechnik) homogenizer in 1X RIPA buffer supplemented with the proteinase inhibitor cocktail listed above. The protein concentration in lysates was determined using the Pierce™ BCA Protein Assay Kit (Thermo Scientific; 23227), bovine serum albumin protein standards, and a microplate reader (Spectramax plus 384) at a wavelength of 562nm. The protein ladder used was BLUeye Prestained Protein Ladder (FroggaBio;

PM007-0500F). 20µg or 25 µg of macrophage protein or 5µg of liver protein was mixed with 1.5µL of 4X Laemmli sample buffer (0.25M Tris-HCl pH=6.8 (25% v/v), 5.375M glycerol (40% v/v), 277mM SDS (8% w/v), 6mM bromophenol blue (0.4% w/v), in double-distilled H_2O (ddH_2O)), 1.5µL 2-mercaptoethanol (5% of final volume) and adjusted to 30µL with 1X RIPA buffer. Samples were loaded on a 10% polyacrylamide gel made from a 40% acrylamide solution (acrylamide:bis-acrylamide ratio of 37.5:1) (BioShop; cat: ACR005). The composition of the 10% polyacrylamide separating gel consisted of the following reagents in ddH_2O: 0.375M Tris, 10% acrylamide:bis-acrylamide (w/v), 0.1% SDS (w/v), 0.1% ammonium persulfate (w/v), 0.04% tetramethylethylenediamine (v/v). The composition of the 5% polyacrylamide stacking gel consisted of the following reagents in ddH_2O: 0.063M Tris, 5% acrylamide:bis-acrylamide (w/v), 0.1% SDS (w/v), 0.1% ammonium persulfate (w/v), 0.08% tetramethylethylenediamine (v/v)). Samples were separated in an SDS-PAGE apparatus filled with running buffer (final concentration of 25.01mM Tris, 192.4 mM glycine, 3.47 mM SDS) at 85V for 15 min followed by 100V for 120min. The separated gel proteins were transferred to a polyvinylidene fluoride (PVDF) membrane (membrane was activated by soaking in methanol for 1 min). The transfer took place in a transferring apparatus filled with transfer buffer (final concentration of 25.01mM Tris, 192.4 mM glycine) at 250mA for 90min in a cold room. Membranes were blocked in 5% skim milk (Carnation; Fat Free Instant Skim Milk Powder) in Tris-buffered saline and Tween-20 (TBS-T) (150 mM NaCl, 20 mM Tris-HCl in ddH_2O, pH=7.6, and 0.1% Tween-20) for 1 hour at room temperature. Membranes were incubated with primary antibody overnight at

4°C, washed 4x5min in TBS-T, incubated with donkey anti-rabbit secondary antibody conjugated to horseradish peroxidase (HRP)-conjugated secondary antibody (1:5000 in blocking solution; Jackson Immunoresearch; cat: 711-035-152) or rabbit anti-goat secondary antibody conjugated to HRP (1:5000 in blocking solution; Jackson Immunoresearch; cat: 305-035-003) for 1h at room temperature and washed 4x5min in TBS-T. Primary antibodies used were: rabbit anti-PDZK1 (targeting the carboxy-terminus of PDZK1; 1:1000 in blocking solution; Invitrogen; cat: PA3-16818), rabbit anti-PDZK1 (targeting the amino-terminus of PDZK1; 1:1000 in blocking solution; Abcam; cat: ab121248), rabbit anti-SR-B1 (1:2000 in blocking solution; Novus biologicals; cat: NB400-104), goat anti-GFP (1:1000 in blocking solution; Abcam; cat: ab6673) and HRP-conjugated rabbit anti-β-actin (1:5000 in blocking solution; Cell Signaling; 5125). Membranes were stripped by washing (2 x 15 min) with stripping buffer (glycine 1.5% w/v, SDS 0.1% w/v, Tween-20 1% v/v, in ddH_2O, pH 2.2). When probing for β-actin, the secondary antibody was not used as the primary antibody was conjugated to HRP. HRP was detected using Clarity Western Enhanced Chemiluminescence Substrate (Bio-Rad) and visualized on a Gel Doc instrument (Bio-Rad; Molecular Imager® ChemiDoc™ XRS+ System; cat: 170-8071).

3.5.Necroptosis

Peritoneal macrophages were seeded on 8-well chamber slides, cultured in DMEM + 10% FBS for 24h then switched to DMEM + 3% newborn calf lipoprotein-deficient serum (NCLPDS) for 24h (to starve the cells of lipoproteins). Cells were treated with either 1) vehicle as a control (DMEM + 3% NCLPDS supplemented with dimethyl

sulfoxide (DMSO) at a final concentration of 1/200, v/v, and 0.01% EDTA (in water) at a final concentration of 1/250, v/v), 2) mouse TNF-α (50 ng/mL) (Gibco; cat: PMC-3014) and z-VAD-FMK (50μM) (APExBIO; cat: A1902), or 3) TNF-α, z-VAD-FMK and human HDL (50 μg/mL) (Athen's Research; cat: 12-16-080412) for 24h in DMEM + 3% NCLPDS. The following day, cells were washed once with cold PBS and stained with a vital dye. As specified in figure captions, cells were either stained with 250μL/well propidium iodide (PI) solution (10 µg PI/mL of PBS) (Sigma-Aldrich; cat: P4170) for 10 min on ice or 100μL/well of 1X SYTOX™ Deep-Red Nucleic Acid Stain (Thermo Fisher; cat: S11380) (1X working solution was made by diluting stock solution 2,000-fold in PBS) and incubated for 30 min at room temperature. Following staining, cells were washed twice with cold PBS and fixed with paraformaldehyde (4% in PBS) for 15 min at room temperature. Following fixation, the chambers on the slides were detached and slides were washed with cold PBS once for 2 min in a Coplin jar. Cell nuclei were counter-stained with 4',6-diamidino-2-phenylindole, dihydrochloride (DAPI; Invitrogen; cat: D1306) (300nM in PBS) for 10 min, washed twice with PBS (2 min per wash), then slides were mounted by adding two drops of Permafluor™ Aqueous Mounting Media (TA-030-FM) or Fluoromount Aqueous Mounting Media (Sigma-Aldrich; cat: F4680) and a cover slip. As specified in figure captions, images were captured with either the Zeiss Axiovert 200M inverted fluorescence microscope (Carl Zeiss Canada Ltd. Toronto, ON, Canada) or the Leica Microsystems STELLARIS-5 confocal microscope (Leica Microsystems, ON, Canada). 5 images were taken per well consisting of different spots (fields of view) in the well (four corners and centre). PI-positive or SYTOX™ Deep-Red-

positive cells were counted using ImageJ (Rasband, W.S., U. S. National Institutes of Health, Bethesda, Maryland, USA). DAPI positive cells were counted using ImageJ. The percentage of necroptotic cells in a field of view was taken as the percentage of PI-positive or SYTOX™ Deep-Red-positive cells; in other words, the PI-positive count or SYTOX™ Deep-Red-positive count divided by the DAPI count x100%.

3.6.Macrophage tdTomato and EGFP fluorescence imaging

Macrophages from *Csf1r-iCre*-positive and *Csf1r-iCre*-negative *Pdzk1*$^{flox/flox}$ *ROSA26*$^{mT/mG}$ were seeded on 8-well chamber slides and cultured as per Methods section 3.3. Cells were washed once with PBS and fixed with paraformaldehyde (2% in PBS) for 20 min at room temperature. The chambers on the slides were detached and slides were washed with PBS once for 3 min in a Coplin jar. Cell nuclei were counter-stained with DAPI (300nM in PBS) for 10 min, washed with PBS once for 3 min, then slides were mounted by adding two drops of Fluoromount Aqueous Mounting Media (Sigma-Aldrich; cat: F4680) and a cover slip. Images were captured using the Leica Microsystems STELLARIS-5 confocal microscope.

3.7.RNA isolation and real time qRT-PCR

Total RNA was extracted from cells or tissues and purified using the RNeasy Mini Kit (Qiagen; cat: 74104) according to the manufacturer's instructions. cDNA was synthesized using the Applied Biosystems™ High-Capacity cDNA Reverse Transcription Kit (Fischer Scientific; cat: 4368814) according to the manufacturer's protocol. 500 or 1000 ng of total RNA was reverse transcribed to cDNA and diluted in ddH_2O to a final concentration of 5ng/μL. Gene expression was measured by real time quantitative

reverse-transcriptase polymerase chain reaction (qRT-PCR) with a single reaction (final volume = 25μL) consisting of 25ng of cDNA, 0.4μM forward primer, 0.4μM reverse primer (primer-pairs listed in Table 1), and 1X SYBR green dye (Invitrogen; cat 11744). *Gapdh* was detected as an internal control. PCR reactions were loaded on an Applied Biosystems™ MicroAmp™ Fast Optical 96-Well Reaction Plate (Fisher Scientific; cat: 4246907) and analysed on the StepOnePlus Real Time PCR system and StepOne Software v2.2.2 (Applied Biosystems, Foster City, CA). The following PCR program was used: holding stage (95°C for 10 min), cycling stage (40 cycles: denaturation- 95°C for 15 seconds; annealing/extension- 60°C for 1 min), melt curve stage (95°C for 15 seconds; 60°C for 1 min to 95°C for 15 seconds at a ramp increment of 0.3°C). The relative amount of *Pdzk1* mRNA to internal control was calculated using the delta-delta Ct method $(2^{-\Delta\Delta Ct})$[59], where Ct (cycle threshold), is calculated by the StepOne software and corresponds to the PCR cycle number where the fluorescence signal of the reaction is distinguishable from the baseline signal. The lower the Ct value, the greater the expression of the target gene. First, we calculated $\Delta Ct = \Delta Ct_{gene} - \Delta Ct_{control}$. Then, we calculated $\Delta\Delta Ct$ = avg. ΔCt (treatment samples) – avg. ΔCt (control samples). An example for peritoneal macrophage experiments: $\Delta\Delta Ct$ = avg. ΔCt (wild type PDZ domain 1) – avg. ΔCt (*Pdzk1*-/- PDZ domain 1). Then $2^{-\Delta\Delta Ct}$ was calculated for each group and provides the relative fold change.

3.8.Endpoint RT-PCR and Sanger sequencing

RNA was collected from macrophages and reverse transcribed to cDNA as described in Methods section 3.7. PCR was conducted using primer-pair (PP)2 forward

with either PP2 reverse, PP3 reverse, PP4 reverse, or PP5 reverse (primer sequences in Table 1). A single PCR reaction with a final volume of 25μL consisted of 25ng of cDNA, 0.4μM forward primer, 0.4μM reverse primer, 1X GoTaq Master Mix (Promega; cat: M7123) in ddH_2O. PCR was conducted in a thermocycler (Eppendorf AG Mastercycler Nexus, Hamburg, Germany) using the following PCR program: step 1 (initial denaturation - 95°C for 2 min), step 2 (40 cycles: denaturation- 95°C for 30 seconds; annealing- 56°C for 30 seconds; extension- 72°C for 90 seconds), step 3 (final extension- 72°C for 5 min). A 1.5% agarose gel was prepared with the following reagents: 1.5g of agarose was dissolved per 100mL of 0.5X tris-acetate-EDTA (TAE) buffer (20mM Tris, 10mM glacial acetic acid, 0.5mM EDTA, in ddH_2O) in a microwave. 5μL of RedSafe gel stain (FroggaBio; cat: 21141) was added per 100mL of TAE buffer and the agarose solution was cast in a mold with a gel comb. 5μL of 100bp DNA ladder (FroggaBio; cat: DM003) and 20 μL of each PCR sample was loaded in the gel and samples were separated in an electrophoresis tank in 0.5X TAE buffer at 90V for 90 min at room temperature. The DNA in the gel was visualized using a gel doc (Bio-Rad; Molecular Imager® Gel Doc™ XR System; cat: 170-8170).

For DNA sequencing, the PCR reaction containing the PCR product was diluted $1/10^{th}$ in ddH_2O and was sent together with corresponding primes to Mobix Laboratory at McMaster University. The nucleotide sequence obtained was examined on NCBI's nucleotide-BLAST program which aligns the query sequence against a database of mouse nucleotide sequences to find matches.

3.9.Statistical analysis

Graphpad Prism (GraphPad Software, San Diego, CA) was used to analyze data. When comparing two groups of data, a normality test (Shapiro-Wilk test) was conducted using Prism. Since sample groups passed the normality test, a parametric student's t-test was used to compare groups, rather than a non-parametric test. When comparing multiple groups, a one-way analysis of variance (ANOVA) test was used with post-hoc Tukey's multiple comparisons test. Data are presented as mean ± standard error of the mean (SEM) and were considered statistically significant if $p < 0.05$.

CHAPTER 4: RESULTS

4.1.PDZK1 detection in human THP-1 monocytes and PMA-stimulated THP-1 cells.

To examine if *PDZK1* is expressed in human macrophages, I first used the human THP-1 monocytic cell line to derive human THP-1 macrophages. Exposure to phorbol 12-myristate 13-acetate (PMA) is known to trigger the differentiation of THP-1 cells from a monocytic to a macrophage-like phenotype[60]. Real time quantitative reverse-transcriptase polymerase chain reaction (qRT-PCR) and Western blotting were performed to assess *PDZK1* mRNA and PDZK1 protein levels, respectively. RNA samples were collected from unstimulated and PMA-stimulated THP-1 cells and assessed by real time qRT-PCR as described in Methods. *PDZK1* mRNA was detected in unstimulated and PMA-stimulated THP-1 cells (Ct values ~23). However, there was no significant difference in *PDZK1* mRNA expression between the two (Figure 2). Immunoblotting with an antibody directed against the carboxy-terminus of PDZK1 revealed the presence of a band migrating at the expected molecular weight (~70kDa) predicted for PDZK1 in PMA-stimulated but not unstimulated THP-1 cells (Supplementary Figure 1A and 1B). These data suggest that PDZK1 protein appears to be induced during differentiation of monocytes to macrophages, but this induction does not involve changes in *PDZK1* mRNA levels.

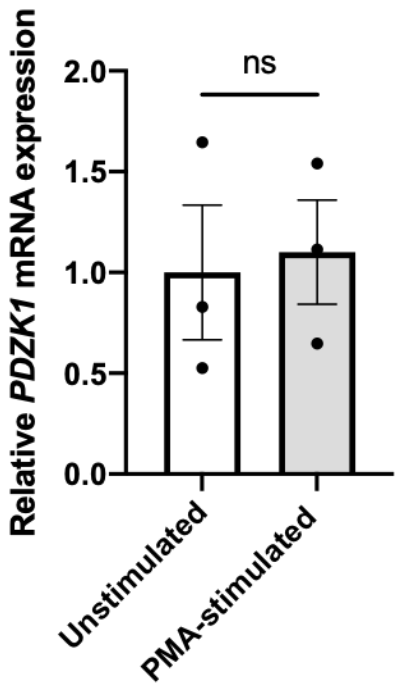

Figure 2: Real time qRT-PCR analysis of *PDZK1* in unstimulated human THP-1 cells and PMA-stimulated THP-1 cells.

THP-1 monocytes were either left untreated or were differentiated for 48h with 100ng/mL of PMA in RPMI. (**A**) RNA was collected, reverse transcribed into cDNA and subjected to real time PCR to assess the relative abundance of the *PDZK1* transcript. Data are expressed as means (relative to unstimulated THP-1 cells normalized to 1) +/- SEM determined by an unpaired student's t-test (N=3 technical replicates per group). NS: not statistically significant ($p>0.05$).

4.2.Western blotting for PDZK1 in mouse peritoneal macrophages

Next, I examined if I could detect PDZK1 protein in thioglycollate-elicited mouse peritoneal macrophages. Cells were collected from C57BL/6J mice and were either 1) lysed immediately following harvesting (to assess *in vivo* levels of PDZK1 protein) (Supplementary Figure 2A, lane 1); 2) cultured in DMEM + 10% FBS for 24h (Supplementary Figure 2A, lane 2); 3) cultured in DMEM + 10% FBS for 24h followed by DMEM + 3% NCLPDS for 24h (Supplementary Figure 2A, lane 3). Western blot analysis using a carboxy-terminal PDZK1 antibody demonstrated that freshly harvested peritoneal macrophages exhibited no detectable band at 70kDa (predicted size of PDZK1), whereas culturing cells for 24h in DMEM + 10 % FBS induced a band at 70kDa, and the intensity of this band was significantly reduced when the cells were cultured for another 24h in a different media consisting of DMEM + 3 % NCLPDS (Supplementary Figure 2B). SR-B1 protein was also assessed as it is known that in certain tissues, such as in the liver, PDZK1 protein stabilizes SR-B1 protein; however, in other tissue types such as endothelial cells and macrophages there is no such influence[22,29,61]. Consistent with the literature, SR-B1 protein levels in macrophages are not influenced by changes in PDZK1 protein levels as observed when comparing lanes 2 and 3 (Supplementary Figure 2C). Interestingly, freshly harvested cells displayed 50% less SR-B1 compared to cultured cells (lanes 2 and 3), which is likely not a result of differences in PDZK1. Rather, this could be because the thioglycollate-elicited peritoneal cavity contains ~55-60% non-macrophage cells[62] that might not express SR-B1.

However, these non-macrophage cells are presumably mostly eliminated during differential adherence used to enrich for macrophages (see Methods).

4.3. Regulation of the 70kDa band detected by the carboxy-terminal PDZK1 antibody in mouse peritoneal macrophages

As observed in Supplementary Figure 2, the 70kDa band detected by the carboxy-terminal PDZK1 antibody in macrophages appears to be significantly affected by culture conditions. However, it was not clear if the decrease in this band (from lane 2 to lane 3 in Supplementary Figure 2) was due to the additional time in culture (24h vs 48h), the reduction in serum concentration (10% to 3%), the switch from fetal to newborn calf serum (NCS), or the presence/absence of lipoproteins. To determine which one of these factors contributed to this decrease, Western blotting was performed on thioglycollate-elicited mouse peritoneal macrophages cultured in either media containing 3% or 10% FBS, NCS, or NCLPDS (Supplementary Figure 3). NCLPDS is derived from NCS by removing lipoproteins from NCS by ultracentrifugation; therefore, using these two serums allows us to test how lipoproteins influence PDZK1 expression. Following harvesting, all macrophages were cultured in DMEM + 10% FBS for 24h. Macrophages were then lysed for protein collection (24h time point) or cultured for an additional 24h in either DMEM + 3% FBS, NCS, or NCLPDS, or DMEM + 10% FBS, NCS, or NCLPDS (Supplementary Figure 3A). The results show that culturing macrophages in 3% FBS, NCS, or NCLPDS resulted in significantly lower levels of the 70kDa band compared to 10% FBS, NCS, or NCLPDS, respectively (Supplementary Figure 3B). There was no significant difference in this band when comparing cells cultured in different serum sources (FBS versus NCS), in the presence or absence of lipoproteins (NCS versus NCLPDS), or for different culture times (24h or 48h in culture). Therefore, serum

concentration significantly affects the band at 70kDa (which is thought to be PDZK1), as opposed to the time in culture, the source of the serum, or the presence/absence of lipoproteins.

To determine if culturing mouse peritoneal macrophages in 3% or 10% serum resulted in differences in the levels of *Pdzk1* transcripts, real time qRT-PCR was conducted to assess *Pdzk1* transcript levels in macrophages cultured in 3% or 10% serum. Cells were cultured for an initial 24h in DMEM + 10% FBS and were either lysed to collect RNA, or cultured for a second 24h in either DMEM + 3% NCLPDS or DMEM + 10% NCLPDS, then lysed to collect RNA. Preliminary results (macrophages from N=2 mice) show no apparent differences in *Pdzk1* mRNA expression between conditions (Figure 3). Therefore, altering serum concentration does not appear to affect *Pdzk1* mRNA levels.

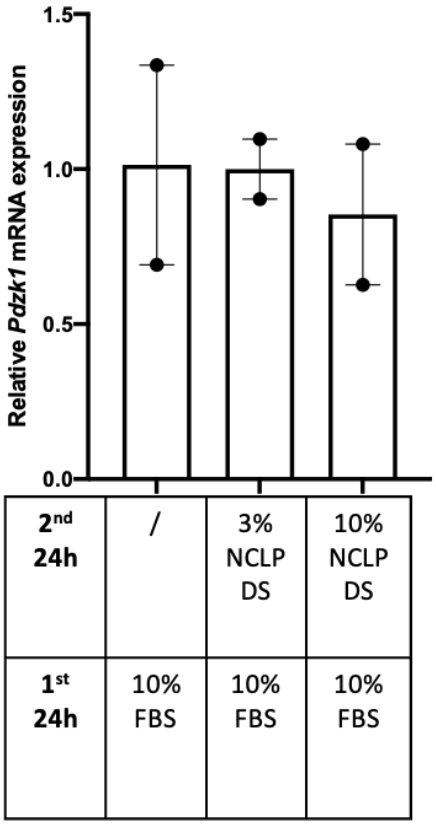

Figure 3: Real time qRT-PCR analysis of *Pdzk1* in wild type mouse peritoneal macrophages under varying culture conditions.

Thioglycollate-elicited peritoneal macrophages were harvested from WT C57BL/6 male mice (N=2) and cultured in DMEM and 10% fetal bovine serum (FBS) for 24h and were either lysed for RNA collection, or cultured for an additional 24h in either DMEM + 3% newborn calf lipoprotein-deficient serum (NCLPDS) or DMEM + 10% NCLPDS. RNA was collected, reverse transcribed into cDNA and subjected to qRT-PCR to assess the relative abundance of the *Pdzk1* transcript. Mean *Pdzk1* mRNA expression (macrophages from N=2 mice) are shown relative to DMEM + 10% FBS (24h only condition) normalized to 1.

4.4.HDL-dependent protection against necroptosis in peritoneal macrophages from *Pdzk1* KO mice

Extensive studies in our laboratory have demonstrated that HDL protects macrophages from necroptosis and that this protection was impaired in macrophages from *Pdzk1-/-* mice (manuscript under review). To confirm PDZK1's involvement in HDL-dependent protection against necroptosis, I performed a necroptosis experiment on macrophages from wild type and *Pdzk1-/-* mice. Thioglycollate-elicited peritoneal macrophages from wild type and *Pdzk1-/-* mice were treated with TNF-α and z-VAD-FMK in the presence or absence of HDL. The combination of TNF-α and z-VAD-FMK promotes necroptosis by activating the necrosome and inhibiting caspases, respectively. Necroptotic cells were stained with propidium iodide (PI) which enters and stains the nucleus of cells with compromised membranes (necroptotic cells) in red. Others from our laboratory have confirmed that the combination of TNF-α + z-VAD-FMK induced necroptosis as indicated by the presence of phospho-MLKL (otherwise not observed in control-treated cells), and that necrostatin-1 (a RIPK1 inhibitor which inhibits necroptosis) was able to inhibit TNF-α + z-VAD-FMK-induced cell death with similar levels of PI staining compared to control-treated cells (manuscript under review).

As expected, treating wild type and *Pdzk1-/-* macrophages with vehicle resulted in no cell death (Figure 4A and 4B). Treatment of macrophages with TNF-α + z-VAD-FMK induced necroptosis in wild type and *Pdzk1-/-* macrophages (~20-30% of cells were PI-positive) (Figure 4C and 4D). However, addition of HDL significantly reduced necroptosis in wild type macrophages but was unable to protect *Pdzk1-/-* macrophages

(Figure 4E and 4F). We believed that this phenotype was a result of a null mutation in *Pdzk1*. To answer this, the following experiments investigated how the *Pdzk1*-targeting mutation affected *Pdzk1* expression in macrophages.

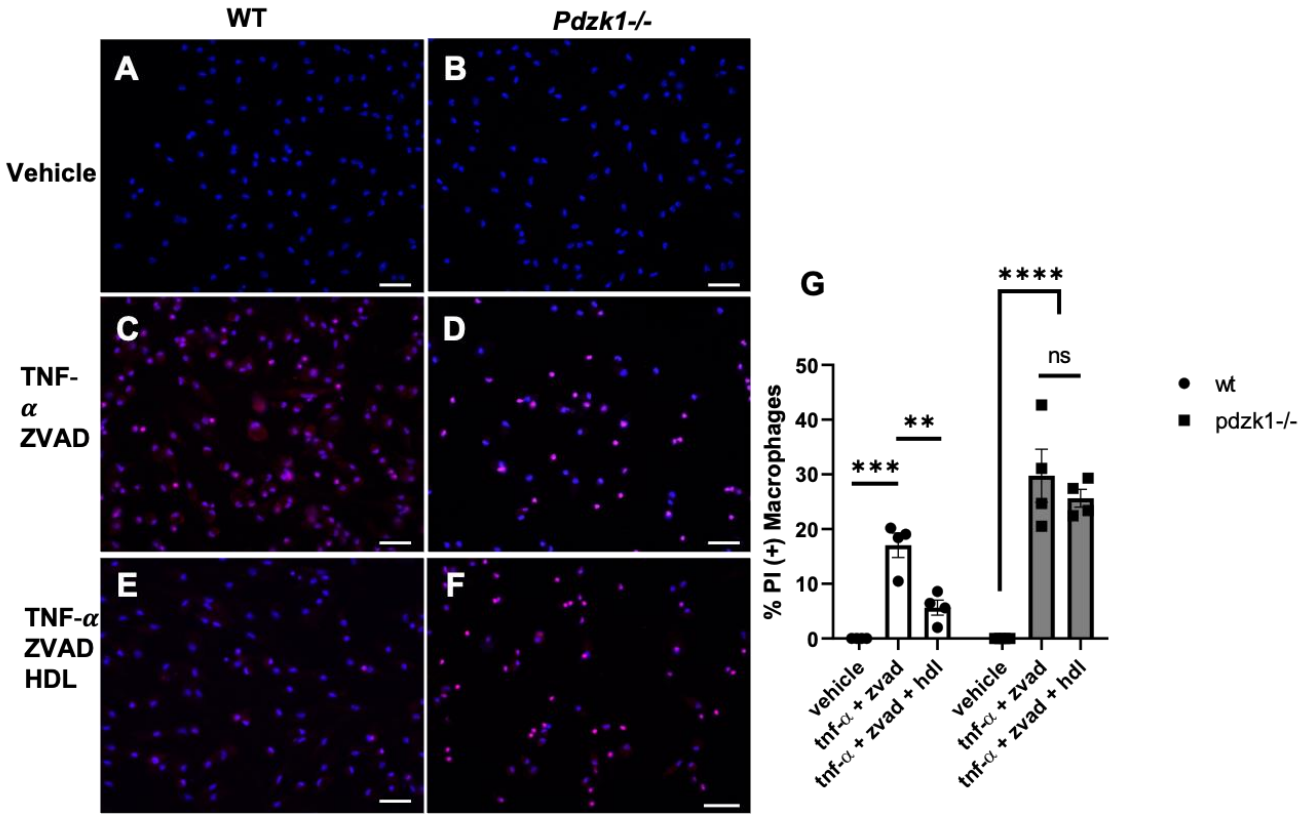

Figure 4: HDL-dependent protection against necroptosis in peritoneal macrophages from wild type and *Pdzk1* KO mice.

Peritoneal macrophages were collected from WT and *Pdzk1-/-* male mice, cultured in DMEM + 10% FBS for 24h, switched to DMEM + 3% NCLPDS for 24h, then treated. Peritoneal macrophages were treated with either vehicle (control), mouse TNF-α (50 ng/mL) and z-VAD-FMK (50μM), or TNF-α, z-VAD-FMK and human HDL (50 μg/mL) for 24 h in DMEM + 3% NCLPDS. Following 24h, cells were stained with propidium iodide (red) to label the nucleus of necroptotic cells, fixed and counterstained with DAPI (blue). Cells were imaged using an inverted fluorescence microscope. Representative images of WT macrophages treated with vehicle (**A**), TNF-α + z-VAD-FMK (**C**), TNF-α + z-VAD-FMK + HDL (**E**) and *Pdzk1-/-* macrophages treated with

vehicle (**B**), TNF-α + z-VAD-FMK (**D**), TNF-α + z-VAD-FMK + HDL (**F**). (**G**) Quantification of the percentage of PI (+) cells (red). Data are means ± SEM determined by one-way ANOVA (N=4 technical replicates per mouse). **p<0.01; ***p<0.001; ****p<0.0001. Scale bars = 20 µm.

4.5.PDZK1 detection in mouse peritoneal macrophages of *Pdzk1* KO mice

Next, I compared *Pdzk1* expression between macrophages from wild type and *Pdzk1* KO mice to investigate how a *Pdzk1*-targeting mutation affects *Pdzk1* expression. The following experiments made use of a mouse strain that harbors a mutation in the *Pdzk1* gene consisting of replacement of exon 2 with a neomycin resistance gene (Figure 15)[56]. I first compared *Pdzk1* mRNA levels in wild type, heterozygous (*Pdzk1+/-)* and *Pdzk1-/-* macrophages. I analyzed mRNA levels by real time qRT-PCR using 5 different *Pdzk1*-specific primer-pairs (herein referred to as Primer Pair (PP)1, 2, 3, 4, 5), where one of the two primers in the pair overlaps with an exon-exon junction on the *Pdzk1* mRNA while the other rests inside an exon (see schematic in Figure 5 and Table 1 for primer-pair information). I was able to detect transcripts in macrophages from wild type mice using all *Pdzk1* primer-pairs (Ct values ranging from mid-to-high 20s depending on the primer pair). Relative to wild type macrophages, there was no detectable *Pdzk1* mRNA in *Pdzk1-/-* macrophages when using PP1 (as expected for a null mutation) (Figure 6). However, there was significantly higher levels of *Pdzk1* mRNA in *Pdzk1-/-* macrophages using PP2,3,4, and 5, which corresponded to increases of approximately 25-, 20-, 15-, and 8-fold, respectively (Figure 6). Heterozygous macrophages displayed intermediate levels between wild type and *Pdzk1-/-* macrophages, as expected.

To determine if longer transcripts are detectable using primers corresponding to *Pdzk1* in the *Pdzk1-/-* macrophages, gel-based analysis of endpoint RT-PCR was performed using a 5' (upstream) primer with different 3' (downstream) reverse primers. In this experiment, PCR was performed using PP2 forward primer and either PP2,3,4, or

5 reverse primers. I detected transcripts of all lengths in *Pdzk1-/-* macrophages, which were more intense than the amplification products in wild type macrophages (Figure 7). This was consistent with the real time qRT-PCR data (Figure 6). The PCR reaction starting from PP2 forward to PP4 reverse in *Pdzk1-/-* macrophages was sequenced. The nucleotide sequence obtained was examined on NCBI's nucleotide-BLAST program and showed 100% sequence identity and coverage with three characterized (curated) mouse *Pdzk1* mRNA transcript variants and two non-curated *Pdzk1* mRNA transcript variants (Figure 8A and 8B).

Next, wild type, *Pdzk1+/-* and *Pdzk1-/-* macrophages were analyzed by Western blotting for the 70kDa band detected by the anti-PDZK1 antibodies. Two different PDZK1 antibodies were used: a polyclonal antibody recognizing the carboxy-terminus of PDZK1 (Invitrogen PA316818) and a polyclonal antibody recognizing the amino-terminus of PDZK1 (generated from a recombinant fragment corresponding to the first 90 amino acids of PDZK1) (see Figure 16 for mouse PDZK1 amino acid sequence). Both antibodies detected a ~70kDa protein in wild type and heterozygous samples (Supplementary Figure 4A). Surprisingly, however, they also detected a similar amount of the corresponding band in *Pdzk1-/-* cells (Supplementary Figure 4A-C).

Table 1: PCR Primers

Primer-pairs (PP)	Primer sequence (5' → 3')	Total base pairs (bp)	Melting temperature*	% GC content	Amplicon size (bp)
ms *Pdzk1* PP1 for.	gacactgatggtcacctgatccg	23	66.2	56.5	139
ms *Pdzk1* PP1 rev.	ccagctccaccacctgcg	18	66.5	72.2	
ms *Pdzk1* PP2 for.	aactatccaaggtaaaaagggtgtg	25	60.8	40	146
ms *Pdzk1* PP2 rev.	tttcaaccacttcctcatggc	21	62.3	47.6	
ms *Pdzk1* PP3 for.	gctgtcaatggcaagtctgtgg	22	65.3	54.5	131
Ms *Pdzk1* PP3 rev.	aaccgagccaggctatagatgc	22	63.9	54.5	
ms *Pdzk1* PP4 for.	tgtcaaagaggtacagcagg	20	56.5	50	131
ms *Pdzk1* PP4 rev.	tgctcttgattctctccacc	20	57.9	50	
ms *Pdzk1* PP5 for.	agcaaaagaccgaactctcagc	22	62.3	50	116
ms *Pdzk1* PP5 rev.	tcggagaggcagttcctgg	19	63.9	63.2	
ms *Gapdh* for.	accacagtccatgccatcac	20	61.9	55	452
ms *Gapdh* rev.	tccaccaccctgttgctgta	20	62.5	55	
hu *PDZK1* for.	atcaaagaggtacagaaggg	20	53	45	131
hu *PDZK1* rev.	ctgctctggattctatccac	20	55	50	
hu *GAPDH* for.	acccagaagactgtggatgg	20	60	55	200
hu *GAPDH* rev	tctagacggcaggtcaggtc	20	60	60	

*Calculated on the Thermo Fischer Scientific website.

A

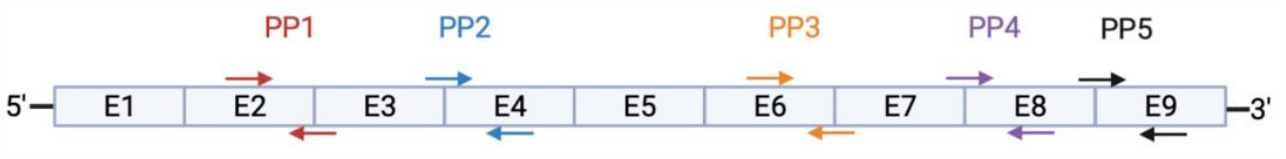

B

```
   1 aatcaatctttgtccaaagtccagtgagttccaagactagtagtgttcacagcggggaga
  61 atttccagtgcggagcggatccttcgccacagaaatggcctccaccttcaacccagaga
 121 gtgtaaattgtccaaacaagaggggcagaactatggcttctttctccgaattgagaagga
 181 cactgatggtcacctgatccgggtgattgaggaggggagcccagcagagaaggcggggct
 241 cctggacggtgacagggtgctcaggatcaatggtgtctttgtcgacaaggaggagcatgc
 301 gcaggtggtggagctggtcagaaagagtgggaattcagtgactctgctggtcctggatgg
 361 agactcctatgagaaggctgtgaaaaatcaggtggatttgaaagagctggatcaaagcca
 421 gagggaggccgctctgaatgataagaaaccgggccctgggatgaacggagcggtggagcc
 481 gtgtgcccagccacggctctgctacctggtgaaggagggcaacagctttggcttctctct
 541 gaaaactatccaaggtaaaaagggtgtgtacttgactaatataatgcctcagggcgtggc
 601 catgaaagctggtgttctggctgatgatcacttgattgaagtgaatggagaaaatgtaga
 661 gaacgccagccatgaggaagtggttgaaaaggtgacaaagtcaggaagccgtatcatgtt
 721 cctccttgtggacaaagaaactgccaggtgccatagtgaacagaagacacaattcaagag
 781 ggagacagccagtttgaaactgctgccccaccagccccgggtggtagtgatcaagaaggg
 841 cagcaatggctatggcttctatctgagggcggggcctgaacagaaaggtcaaatcattaa
 901 ggacatagaacccgggagcccagcagaggcagctggcttgaagaacaatgacttggtagt
 961 tgctgtcaatggcaagtctgtggaagctcttgatcatgacggtgtggtggaaatgattag
1021 aaaaggtggagaccagactactctgttggtgctggacaaagaggcagagagcatctatag
1081 cctggctcggttctctccacttctttactgccaaagtcaagaactgcctaatggttctgt
1141 caaggaaggcccagctccgatccctgctcctctggaggccacaggctcagagcccacaga
1201 ggacgcggagggtcacaagcccaagctctgcaggctgcttaaagaggacgatagctacgg
1261 ctttcacctgaatgccattcggggtcagcctggctcctttgtcaaagaggtacagcaggg
1321 tggccctgctgacaaggctgggctggagaatgaggacgtcatcatcgaagtgaacgggga
1381 gaacgtgcaagaggaaccctacgacagagtggtggagagaatcaagagcagcgggaagca
1441 cgtcactctgttggtctgtggaaagatggcctacagctacttccaagctaagaaaatccc
1501 catcgtttcctccatggccgagcccctggtggctggccctgatgaaaaaggagagacgtc
1561 tgcggagtccgagcatgacgcccacccagcaaaagaccgaactctcagcacagcctcgca
1621 ctcttcgtctaactctgaagacacggagatgtgaagagaacaaatgatgcttcctcttga
1681 gggcccaggaactgcctctccgaggaatgagccctgccgaccccgtcagacctcctctgg
1741 accatctgtcccccagactgtctgttgttgtaagggctgctactgcaggttgcttattta
1801 agctcaacttagccagaggagggaccaggttcagggtctttctatgtggtatcttccaaa
1861 gtgcaacttttcacttctgttgatgagacctcttccttctgcaggcttgagcacctggga
1921 tgattcactgtccatgtgagcgctgctaatttaaagaatcaagcagatgcctgttatagaa
1981 gtgtgcttttgtagcaatgctgtggctgagcagcattgctaagtgcttctgagttgtttg
2041 caacttccctgttggctaatagaatccgaatagtgtctttgttccatacaaacatttcat
2101 gctttctcatttgcttccagaagcccaaaacatgcaaaatacacactgtggtcttagtaa
2161 taaagggaggcttccaggaaatatacttcagcattttcttatgttacatttgagtattaa
2221 aaaaaaacctcaacaccttccttttactgtcggagggcttatgtttcagaacaggaaagg
2281 gcttgttccagttaacgtctacctccagcgctgaggcagagggaaagccaacccgagcca
2341 gccactgctggattagcacggaacattcactcttctctaatttaagaggaaataaagatt
2401 ggtatacctaaaatcta
```

Figure 5: *Pdzk1* mRNA transcript and mouse primer-pairs.

A) Schematic representation of the *Pdzk1* mRNA transcript composed of 9 exons with the locations in which each primer-pair (PP) hybridizes to on the transcript. For each primer-pair, one of the primers hybridizes to (overlaps with) an exon-exon junction while the other primer hybridizes to a sequence within an exon. **B**) The nucleotide sequence of mouse *Pdzk1* mRNA transcript variant 1. The sequence is annotated to highlight start and stop codons (bolded and underlined), four PDZ domains (PDZ1 in red, PDZ2 in blue, PDZ3 in orange and PDZ4 in purple), exon-exon boundaries (shaded in yellow; an intron lies between the two shaded nucleotides), and primer-pair sequences from table 1 (shaded in gray). The only difference between the three characterized *Pdzk1* transcript variants is the 5' untranslated region; there are three alternative exons that can be used for the 5' untranslated region.

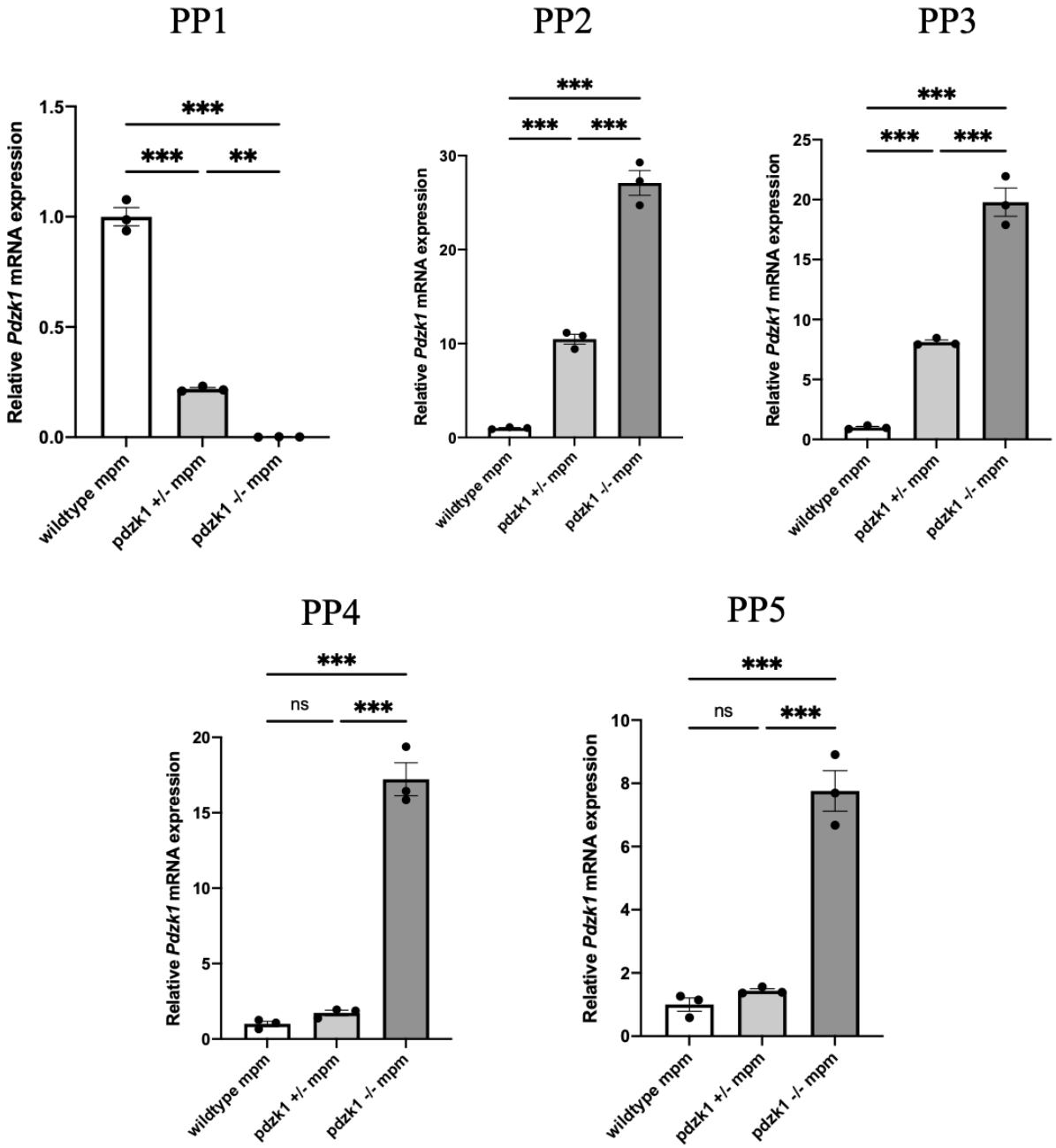
PP1
PP2
PP3
PP4
PP5
Relative Pdzk1 mRNA expression
wildtype mpm
pdzk1 +/- mpm
pdzk1 -/- mpm
***
**
ns

Figure 6: *Pdzk1* mRNA expression in WT, *Pdzk1*+/- and *Pdzk1*-/- mouse peritoneal macrophages.

Thioglycollate-elicited peritoneal macrophages from a WT C57BL/6J, *Pdzk1*+/- and *Pdzk1*-/- male mouse were harvested and cultured for 3 days in DMEM + 10% FBS. RNA was collected, reverse transcribed into cDNA and subjected to real time PCR. Five unique PDZK1 primer-pairs (PP1,2,3,4, and 5) were used to assess the presence and relative abundance of the *Pdzk1* mRNA transcript. Data are expressed as means (relative to WT normalized to 1) +/- SEM determined by one-way ANOVA (N=3 technical replicates per mouse). NS: not statistically significant ($p>0.05$); **$p<0.01$; ***$p<0.001$.

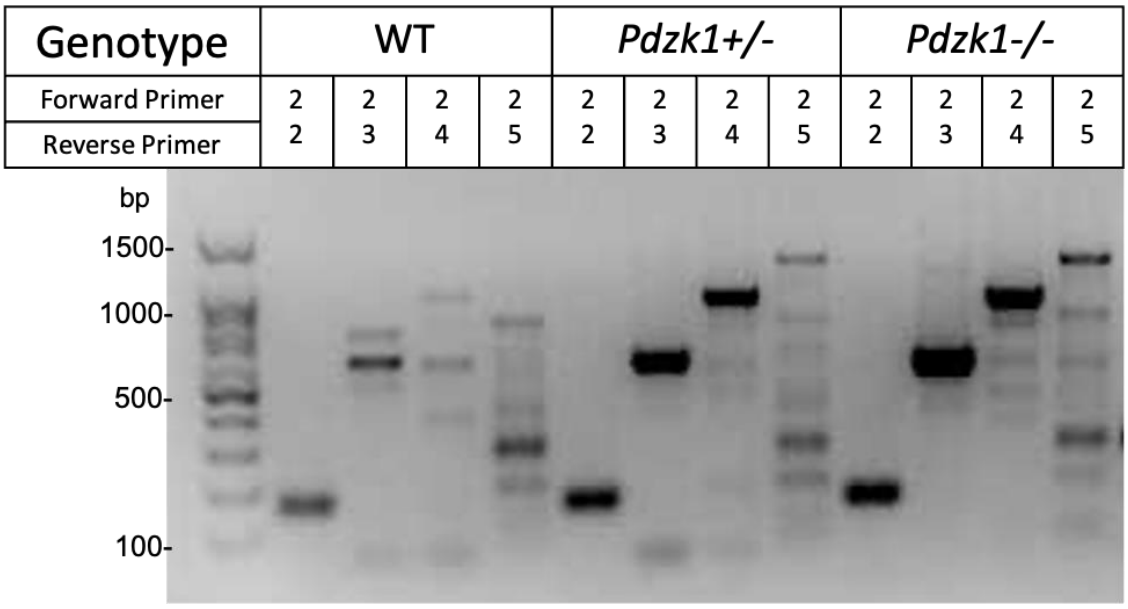

Figure 7: Gel-based analysis of endpoint RT-PCR of *Pdzk1* mRNA from WT, *Pdzk1+/-* and *Pdzk1-/-* mouse peritoneal macrophages.

Thioglycollate-elicited peritoneal macrophages from WT C57BL/6J, *Pdzk1*+/- and *Pdzk1-/-* male mice were harvested and cultured for 3 days in DMEM + 10% FBS. RNA was collected, reverse transcribed into cDNA and subjected to PCR and agarose gel electrophoresis. cDNA samples were amplified by PCR using primer-pair (PP)2 forward primer with either PP2 reverse, PP3 reverse, PP4 reverse, or PP5 reverse primers, which produce 146bp, 549bp, 887bp, and 1160bp products, respectively. PCR samples were separated by agarose gel (1.5%) electrophoresis. A 1kbp DNA ladder was used.

A

Description	Scientific Name	Max Score	Total Score	Query Cover	E value	Per. Ident	Acc. Len	Accession
Transcripts								
PREDICTED: Mus musculus PDZ domain containing 1 (Pdzk1), transcript variant X2, mRNA	Mus musculus	1557	1557	100%	0.0	100.00%	2695	XM_011240178.3
PREDICTED: Mus musculus PDZ domain containing 1 (Pdzk1), transcript variant X1, mRNA	Mus musculus	1557	1557	100%	0.0	100.00%	2488	XM_017319675.2
Mus musculus PDZ domain containing 1 (Pdzk1), transcript variant 3, mRNA	Mus musculus	1557	1557	100%	0.0	100.00%	2673	NM_001355710.1
Mus musculus PDZ domain containing 1 (Pdzk1), transcript variant 2, mRNA	Mus musculus	1557	1557	100%	0.0	100.00%	2371	NM_001146001.2
Mus musculus PDZ domain containing 1 (Pdzk1), transcript variant 1, mRNA	Mus musculus	1557	1557	100%	0.0	100.00%	2417	NM_021517.3

B

Mus musculus PDZ domain containing 1 (Pdzk1), transcript variant 1, mRNA.

Sequence ID: NM_021517.3 **Length:** 2417 **Number of Matches:** 1

Range 1: 582 to 1424 GenBank Graphics ▼ Next Match ▲ Previous Match

Score	Expect	Identities	Gaps	Strand
1557 bits(843)	0.0	843/843(100%)	0/843(0%)	Plus/Plus

```
Query  1     TAATGCCTCAGGGCGTGGCCATGAAAGCTGGTGTTCTGGCTGATGATCACTTGATTGAAG  60
             ||||||||||||||||||||||||||||||||||||||||||||||||||||||||||||
Sbjct  582   TAATGCCTCAGGGCGTGGCCATGAAAGCTGGTGTTCTGGCTGATGATCACTTGATTGAAG  641

Query  61    TGAATGGAGAAAATGTAGAGAACGCCAGCCATGAGGAAGTGGTTGAAAAGGTGACAAAGT  120
             ||||||||||||||||||||||||||||||||||||||||||||||||||||||||||||
Sbjct  642   TGAATGGAGAAAATGTAGAGAACGCCAGCCATGAGGAAGTGGTTGAAAAGGTGACAAAGT  701

Query  121   CAGGAAGCCGTATCATGTTCCTCCTTGTGGACAAAGAAACTGCCAGGTGCCATAGTGAAC  180
             ||||||||||||||||||||||||||||||||||||||||||||||||||||||||||||
Sbjct  702   CAGGAAGCCGTATCATGTTCCTCCTTGTGGACAAAGAAACTGCCAGGTGCCATAGTGAAC  761

Query  181   AGAAGACACAATTCAAGAGGGAGACAGCCAGTTTGAAACTGCTGCCCCACCAGCCCCGGG  240
             ||||||||||||||||||||||||||||||||||||||||||||||||||||||||||||
Sbjct  762   AGAAGACACAATTCAAGAGGGAGACAGCCAGTTTGAAACTGCTGCCCCACCAGCCCCGGG  821

Query  241   TGGTAGTGATCAAGAAGGGCAGCAATGGCTATGGCTTCTATCTGAGGGCGGGGCCTGAAC  300
             ||||||||||||||||||||||||||||||||||||||||||||||||||||||||||||
Sbjct  822   TGGTAGTGATCAAGAAGGGCAGCAATGGCTATGGCTTCTATCTGAGGGCGGGGCCTGAAC  881

Query  301   AGAAAGGTCAAATCATTAAGGACATAGAACCCGGGAGCCCAGCAGAGGCAGCTGGCTTGA  360
             ||||||||||||||||||||||||||||||||||||||||||||||||||||||||||||
Sbjct  882   AGAAAGGTCAAATCATTAAGGACATAGAACCCGGGAGCCCAGCAGAGGCAGCTGGCTTGA  941

Query  361   AGAACAATGACTTGGTAGTTGCTGTCAATGGCAAGTCTGTGGAAGCTCTTGATCATGACG  420
             ||||||||||||||||||||||||||||||||||||||||||||||||||||||||||||
Sbjct  942   AGAACAATGACTTGGTAGTTGCTGTCAATGGCAAGTCTGTGGAAGCTCTTGATCATGACG  1001

Query  421   GTGTGGTGGAAATGATTAGAAAAGGTGGAGACCAGACTACTCTGTTGGTGCTGGACAAAG  480
             ||||||||||||||||||||||||||||||||||||||||||||||||||||||||||||
Sbjct  1002  GTGTGGTGGAAATGATTAGAAAAGGTGGAGACCAGACTACTCTGTTGGTGCTGGACAAAG  1061

Query  481   AGGCAGAGAGCATCTATAGCCTGGCTCGGTTCTCTCCACTTCTTTACTGCCAAAGTCAAG  540
             ||||||||||||||||||||||||||||||||||||||||||||||||||||||||||||
Sbjct  1062  AGGCAGAGAGCATCTATAGCCTGGCTCGGTTCTCTCCACTTCTTTACTGCCAAAGTCAAG  1121

Query  541   AACTGCCTAATGGTTCTGTCAAGGAAGGCCCAGCTCCGATCCCTGCTCCTCTGGAGGCCA  600
             ||||||||||||||||||||||||||||||||||||||||||||||||||||||||||||
Sbjct  1122  AACTGCCTAATGGTTCTGTCAAGGAAGGCCCAGCTCCGATCCCTGCTCCTCTGGAGGCCA  1181

Query  601   CAGGCTCAGAGCCCACAGAGGACGCGGAGGGTCACAAGCCCAAGCTCTGCAGGCTGCTTA  660
             ||||||||||||||||||||||||||||||||||||||||||||||||||||||||||||
Sbjct  1182  CAGGCTCAGAGCCCACAGAGGACGCGGAGGGTCACAAGCCCAAGCTCTGCAGGCTGCTTA  1241

Query  661   AAGAGGACGATAGCTACGGCTTTCACCTGAATGCCATTCGGGGTCAGCCTGGCTCCTTTG  720
             ||||||||||||||||||||||||||||||||||||||||||||||||||||||||||||
Sbjct  1242  AAGAGGACGATAGCTACGGCTTTCACCTGAATGCCATTCGGGGTCAGCCTGGCTCCTTTG  1301

Query  721   TCAAAGAGGTACAGCAGGGTGGCCCTGCTGACAAGGCTGGGCTGGAGAATGAGGACGTCA  780
             ||||||||||||||||||||||||||||||||||||||||||||||||||||||||||||
Sbjct  1302  TCAAAGAGGTACAGCAGGGTGGCCCTGCTGACAAGGCTGGGCTGGAGAATGAGGACGTCA  1361

Query  781   TCATCGAAGTGAACGGGGAGAACGTGCAAGAGGAACCCTACGACAGAGTGGTGGAGAGAA  840
             ||||||||||||||||||||||||||||||||||||||||||||||||||||||||||||
Sbjct  1362  TCATCGAAGTGAACGGGGAGAACGTGCAAGAGGAACCCTACGACAGAGTGGTGGAGAGAA  1421

Query  841   TCA  843
             |||
Sbjct  1422  TCA  1424
```

Figure 8: Nucleotide BLAST of Sanger sequencing mRNA product.

PCR was performed on cDNA from peritoneal macrophages of a *Pdzk1-/-* mouse using PP2 forward primer and PP4 reverse primer and the amplification product was sequenced via Sanger method using the same primers. The output sequence was aligned against a database of mouse nucleotide sequences using NCBI's nucleotide-BLAST program. **A)** Five alignments were generated by the BLAST algorithm, depicting alignment scores, sequence coverage, and percent identity. **B)** Alignment of the sequence of the PCR product (Query) with Mus musculus *Pdzk1* mRNA transcript variant 1 (Sbjct). The alignment demonstrates that 100% of the Query is 100% identical to nucleotides 582-1422 of Mus musculus *Pdzk1* mRNA transcript variant 1.

4.6.PDZK1 detection in liver and kidney of *Pdzk1* KO mice

Seeing that I detected PCR products corresponding to *Pdzk1* by real time qRT-PCR and endpoint RT-PCR as well as protein corresponding to the size of PDZK1 by immunoblotting in macrophages from *Pdzk1-/-* mice, I wanted to examine *Pdzk1* transcript and protein levels in liver and kidney from wild type and *Pdzk1-/-* mice. Both liver and kidney highly express *Pdzk1* and there is a lot of research using these *Pdzk1-/-* mice as a model to study PDZK1's role in liver and kidney physiology/pathophysiology[56,63–65]. I assessed expression of *Pdzk1* in livers of wild type and *Pdzk1-/-* mice by real time qRT-PCR. All five primer-pairs amplified products in the livers of wild type mice suggesting the presence of *Pdzk1* transcript. Relative to wild type liver, there was no *Pdzk1* mRNA detected in *Pdzk1-/-* liver when using PP1, 4, and 5, and overexpression of 20-fold and 10-fold when using PP2 and PP3, respectively (Figure 9).

Wild type, *Pdzk1+/-* and *Pdzk1-/-* livers were also analyzed by SDS-PAGE/Western blotting. Both PDZK1 antibodies detected a band of an apparent molecular weight of 70kDa in extracts from wild type liver. This band was absent in extracts from *Pdzk1-/-* liver when the antibody targeting the carboxy-terminal region of PDZK1 was used and reduced in *Pdzk1-/-* liver when the antibody targeting the amino-terminal region of PDZK1 was used (Supplementary Figure 5). Both antibodies detected a corresponding band of intermediate intensity in extracts from livers of *Pdzk1+/-* mice (Supplementary Figure 5).

I also sought to assess how the *Pdzk1*-targeting mutation affected expression of *Pdzk1* in the kidney of *Pdzk1-/-* mice. All five primer-pairs amplified products in the

kidneys of wild type mice suggesting the presence of *Pdzk1* transcript (Figure 10). However, using mRNA prepared from kidneys of *Pdzk1-/-* mice, PP1 did not detect transcript, PP4 and PP5 detected significantly less transcript relative to wild type (reduced by 85% for both primer-pairs), and PP2 and PP3 detected 80-fold and 25-fold higher levels of transcript than samples from wild type kidneys (Figure 10). These results resemble what was seen for liver tissue.

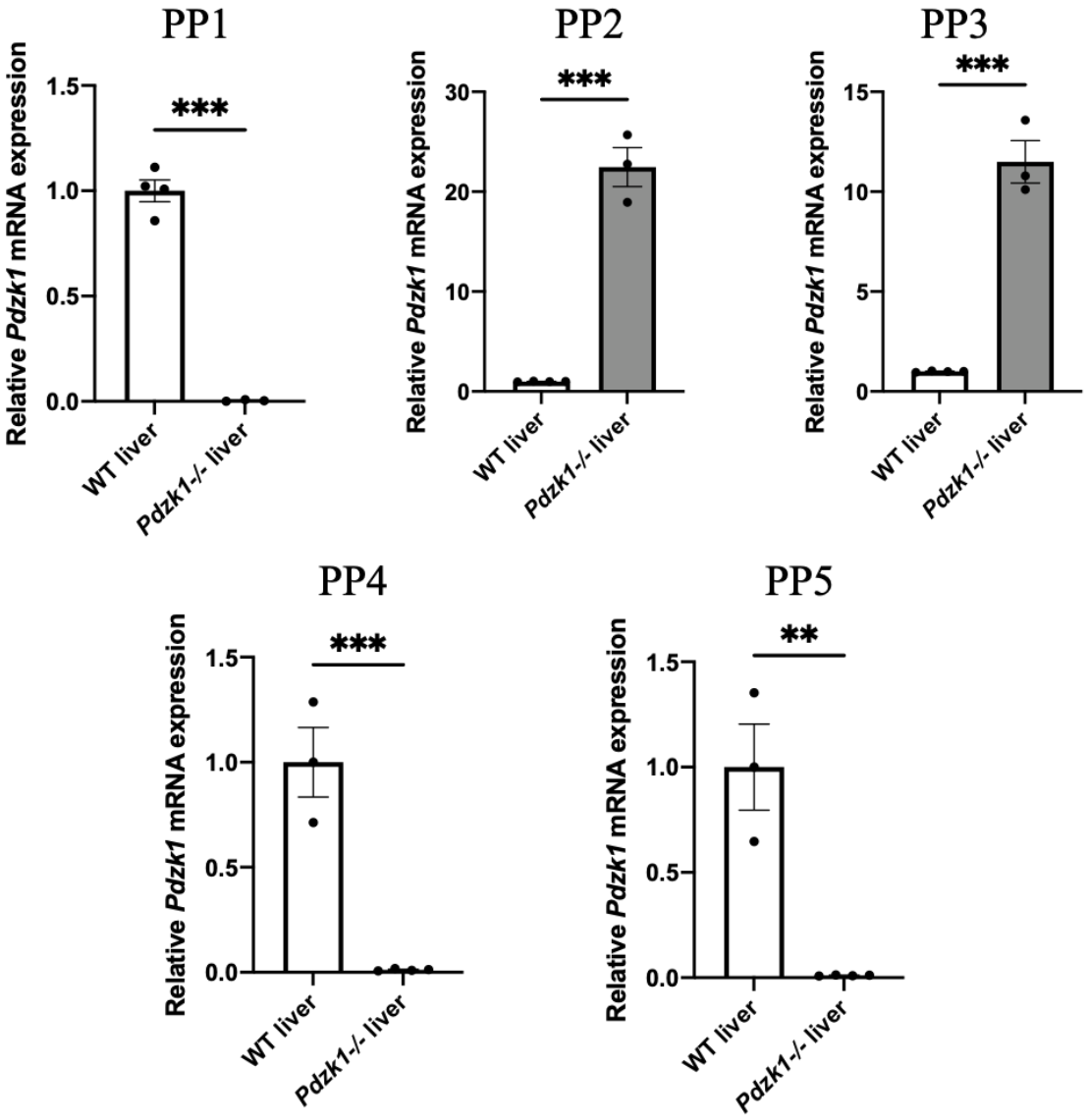

Figure 9: Real time qRT-PCR analysis of *Pdzk1* in WT and *Pdzk1-/-* liver.

The large lobe of livers from WT C57BL/6J and *Pdzk1-/-* male mice were harvested, RNA was collected, reverse transcribed into cDNA and subjected to real time PCR. Five unique *Pdzk1* primer-pairs (PP1,2,3,4, and 5) were used to assess the presence and relative abundance of the *Pdzk1* mRNA transcript. Data are expressed as means

(relative to WT normalized to 1) +/- SEM determined by one-way ANOVA (livers from N=3 or N=4 mice).

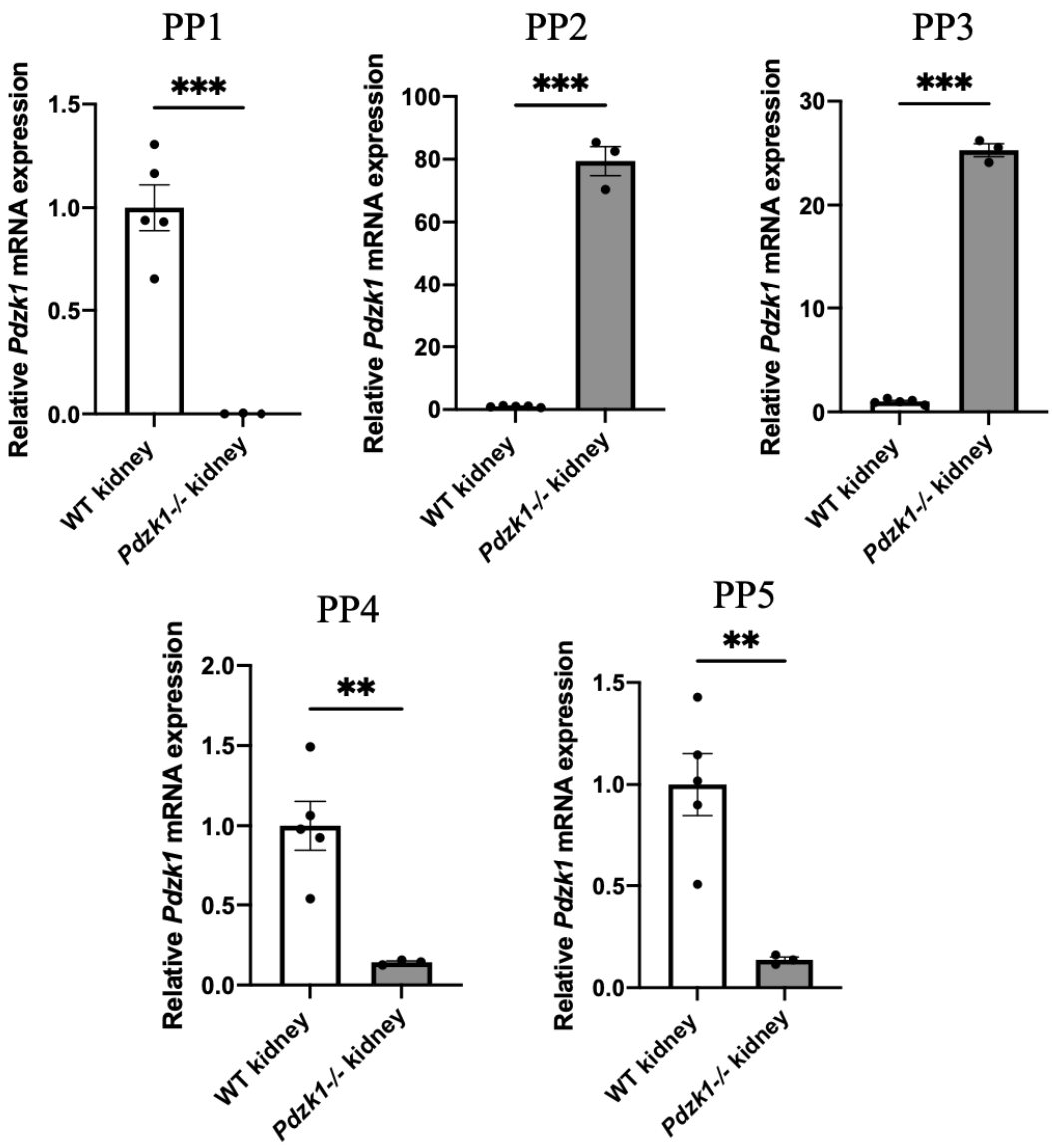

Figure 10: Real time qRT-PCR analysis of *Pdzk1* mRNA in kidney of WT and *Pdzk1-/-* mice.

A piece of the right kidney of WT C57BL/6J and *Pdzk1-/-* male mice was homogenized and the RNA purified. The RNA was reverse transcribed into cDNA and subjected to real time PCR. Five unique *Pdzk1* primer-pairs (PP1,2,3,4, and 5) were used

to assess the presence and relative abundance of the *Pdzk1* mRNA transcript. Data are expressed as means (relative to WT normalized to 1) +/- SEM determined by one-way ANOVA (kidneys from N=3 or N=5 mice).

4.7.Cre-mediated conditional knockout of PDZK1 in mouse peritoneal macrophages

Another targeted method for gene inactivation is through the Cre-loxP system. Our laboratory has purchased different strains of mice (refer to Methods) to develop the following *Csf1r-iCre Pdzk1*$^{flox/flox}$ *ROSA26*$^{mT/mG}$ mouse. This mouse strain is homozygous for a *ROSA26*$^{mT/mG}$ mutation, which consists of a floxed *mT* gene cassette (encoding membrane-targeted tdTomato protein, fluorescing in red) followed by a downstream *mG* cassette (encoding the membrane-targeted EGFP protein, fluorescing in green). In this fluorescent reporter system, tdTomato expression from the *mT* cassette is widespread in cells/tissues. However, Cre-expressing/activated tissues have the *mT* cassette removed enabling expression of the downstream *mG* cassette coding for EGFP. This mouse strain also expresses the tamoxifen-inducible Mer-iCre-Mer fusion protein (Cre protein fused to two mutated murine estrogen receptor ligand-binding domains) under control of the macrophage-specific mouse *Csf1r* (colony stimulating factor 1 receptor) promoter. When tamoxifen is present, tamoxifen binds to the mutated murine estrogen receptor ligand-binding domains on Mer-iCre-Mer allowing Mer-iCre-Mer to translocate to the nucleus where it deletes sequences that are flanked by *loxP* sites in the same orientation. This includes deletion of exons 2 and 3 of *Pdzk1* and deletion of the *mT* cassette allowing for expression of the downstream mG cassette. Therefore, macrophages from tamoxifen-treated Cre-positive mice should lose *Pdzk1* expression and fluoresce green.

Thioglycollate-elicited peritoneal macrophages from vehicle-treated or tamoxifen-treated Cre-positive and Cre-negative mice were examined by confocal microscopy to

assess the proportion of cells that were red-fluorescent or green-fluorescent (Figure 11A). As expected, most cells from tamoxifen-treated Cre-positive mice were green-fluorescent (~85% of cells) while cells from control mice (mice that were either not treated with tamoxifen and/or did not express iCre) displayed virtually no green fluorescence (Figure 11B). Instead, nearly all cells from control mice were red-fluorescent while around 15% of the cells in the macrophage preparation from tamoxifen-treated Cre-positive mice were red-fluorescent (Figure 11C).

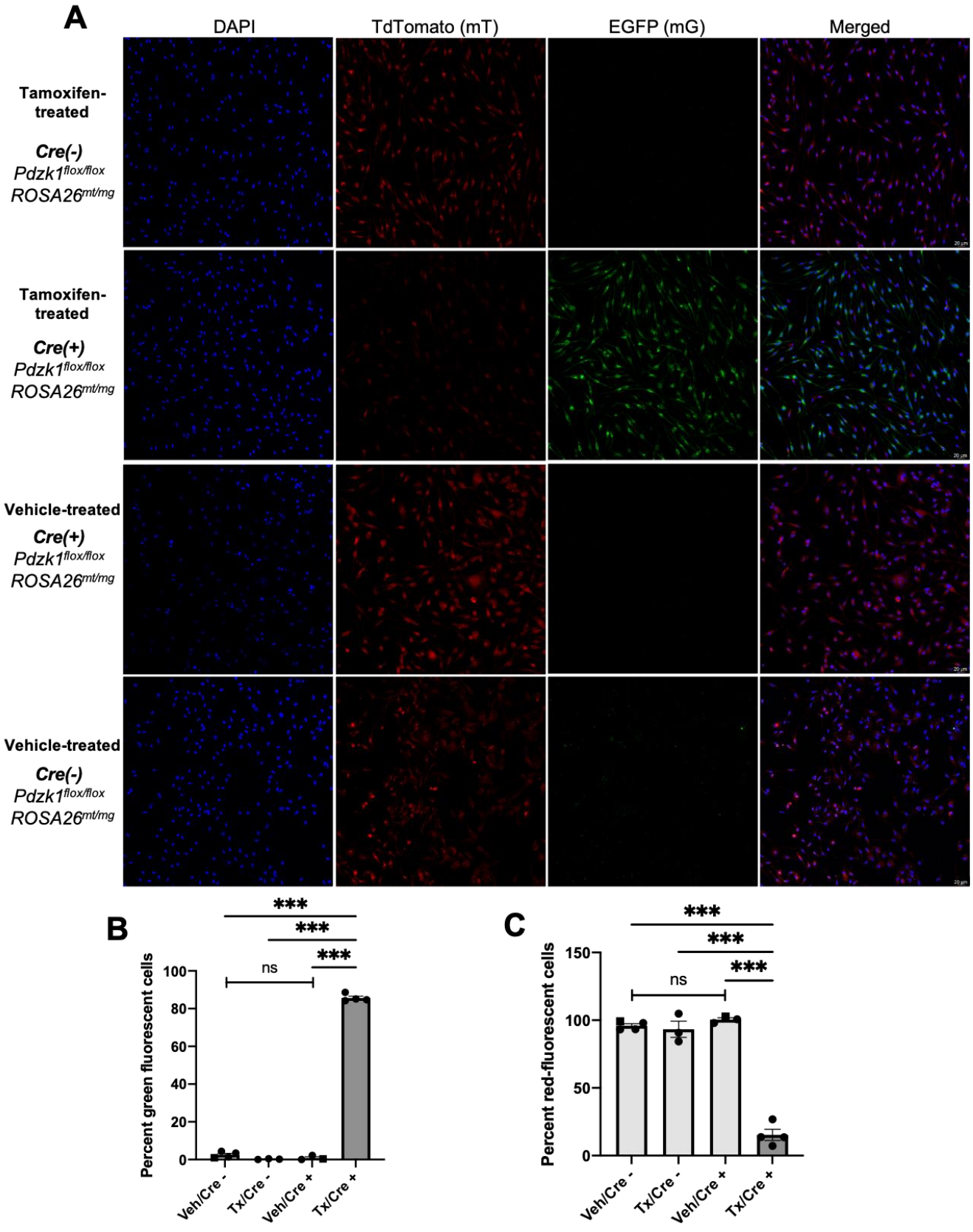
A
DAPI
TdTomato (mT)
EGFP (mG)
Merged
Tamoxifen-treated
Cre(-)
Pdzk1flox/flox
ROSA26mt/mg
Tamoxifen-treated
Cre(+)
Pdzk1flox/flox
ROSA26mt/mg
Vehicle-treated
Cre(+)
Pdzk1flox/flox
ROSA26mt/mg
Vehicle-treated
Cre(-)
Pdzk1flox/flox
ROSA26mt/mg
B
Percent green fluorescent cells
100
80
60
40
20
0
ns
***
***
***
Veh/Cre -
Tx/Cre -
Veh/Cre +
Tx/Cre +
C
Percent red-fluorescent cells
150
100
50
0
ns
***
***
***
Veh/Cre -
Tx/Cre -
Veh/Cre +
Tx/Cre +

Figure 11: tdTomato and EGFP fluorescence in mouse peritoneal macrophages from *Csf1r-iCre Pdzk1$^{flox/flox}$ ROSA26$^{mT/mG}$* mice.

Csf1r-iCre (+) and *Csf1r-iCre* (-) *Pdzk1$^{flox/flox}$ ROSA26$^{mT/mG}$* mice were injected intra-peritoneally for 5 consecutive days with 166mg of tamoxifen (Tx) per kg of mouse to induce Cre activity, or an equivalent volume of vehicle (Veh; corn oil). Thioglycollate-elicited peritoneal macrophages were harvested one week following the last injection and seeded on 8-well chamber slides. Cells were fixed and nuclei were stained with DAPI. Cells were imaged using a confocal microscope with representative images of cells shown for all four groups. Quantification of the percentage of EGFP-positive (green-fluorescent) cells (**B**) and tdTomato-positive (red-fluorescent) cells (**C**) are expressed as means +/- SEM determined by one-way ANOVA (macrophages from N=3 or N=4 mice per genotype; all mice were males except for two mice represented as square data points). **p<0.01, ***p<0.001.

4.7.1. *Pdzk1* mRNA expression in peritoneal macrophages from *Csf1r-iCre* *Pdzk1$^{flox/flox}$ ROSA26$^{mT/mG}$* mice

Next, I assessed *Pdzk1* mRNA expression by real time qRT-PCR in thioglycollate-elicited peritoneal macrophages from *Csf1r-iCre*-positive and *Csf1r-iCre*-negative *Pdzk1$^{flox/flox}$ ROSA26$^{mT/mG}$* mice treated with tamoxifen or vehicle to see if the *Pdzk1* transcript was reduced using all primer-pairs. Results showed a significant reduction using all primer-pairs (PP1-5) (Figure 12). Relative to the *Pdzk1* levels in vehicle-treated Cre-negative control cells, *Pdzk1* transcript in tamoxifen-treated Cre-positive cells was reduced by 80%, 50%, 50%, 80%, and 80% as reflected by PP1,2,3,4, and 5, respectively. This was in line with the fluorescence data (Figure 11) which showed that ~85% of cells from tamoxifen-treated Cre-positive mice were green-fluorescent.

I carried out a similar endpoint RT-PCR experiment as in Figure 7 using PP2 forward primer and PP4 reverse primer on macrophages from tamoxifen-treated Cre-positive mice and controls (Figure 13). As expected, the intensity of the band at 887bp (expected size for the amplification product) was reduced in tamoxifen-treated Cre-positive mice in comparison to the tamoxifen-treated control (reduced by ~70%) and vehicle-treated controls (reduced by ~60%). These data indicate that *Pdzk1* mRNA transcripts were reduced in macrophages from tamoxifen-treated Cre-positive mice compared to controls.

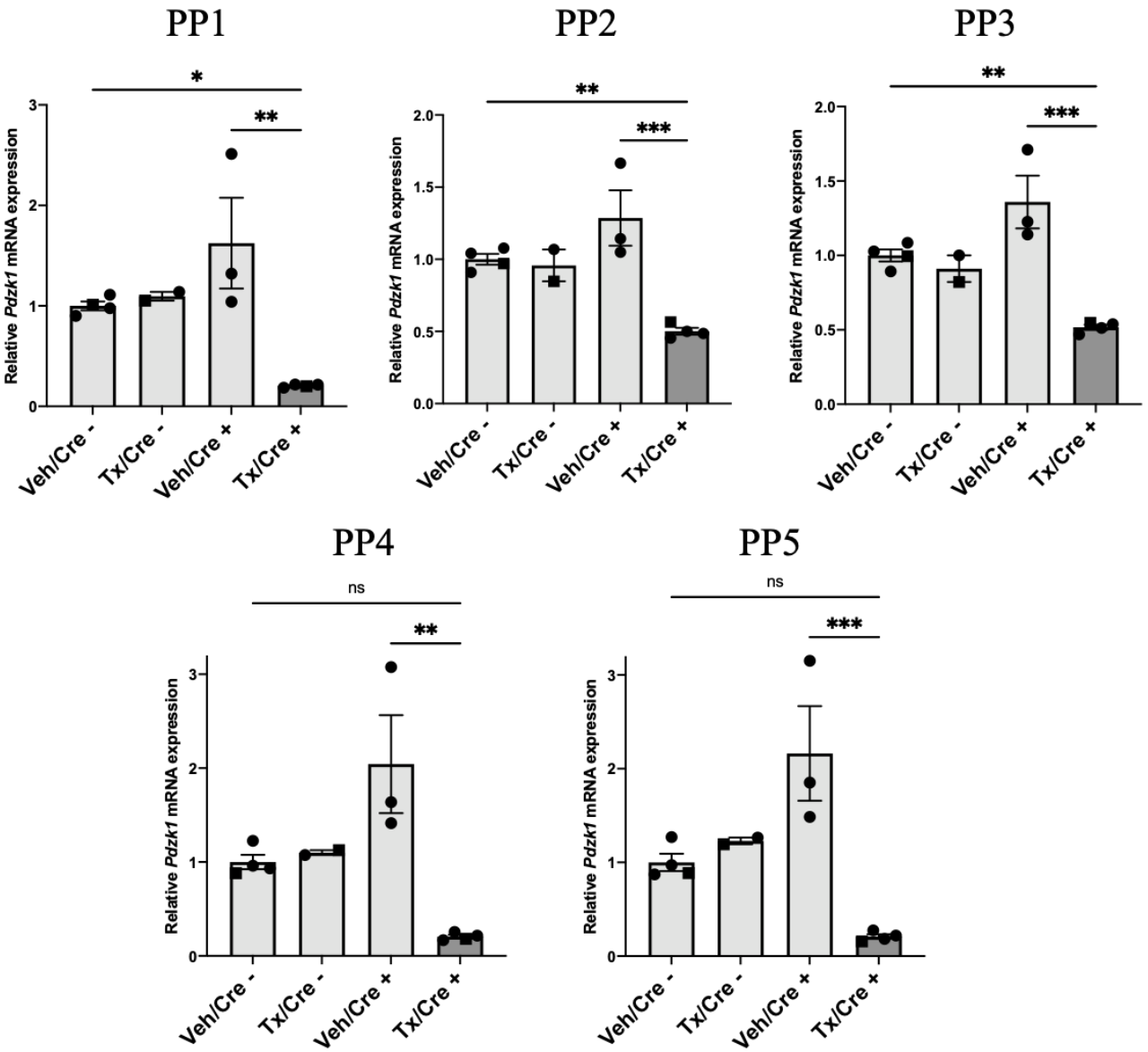

Figure 12: *Pdzk1* mRNA expression in macrophages from *Csf1r-iCre Pdzk1$^{flox/flox}$ ROSA26$^{mT/mG}$* mice.

Csf1r-iCre (+) and *Csf1r-iCre* (-) *Pdzk1$^{flox/flox}$ ROSA26$^{mT/mG}$* mice were injected intra-peritoneally for 5 consecutive days with 166mg of tamoxifen (Tx) per kg of mouse to induce Cre activity, or an equivalent volume of vehicle (Veh; corn oil). Thioglycollate-

elicited peritoneal macrophages were harvested one week following the last injection and cultured for 3 days in DMEM and 10% FBS. RNA was collected, reverse transcribed into cDNA and subjected to real time PCR. Five unique *Pdzk1* primer-pairs (PP1,2,3,4, and 5) were used to assess the presence and relative abundance of the *Pdzk1* mRNA transcript. Expression is relative to *Csf1r-iCre* (-) mice injected with vehicle (normalized to 1). Data are expressed as means +/- SEM determined by one-way ANOVA with Tukey's multiple comparisons test (macrophages from N=2 to N=4 mice per genotype; all mice were males except for three mice represented as square data points). NS: not statistically significant ($p>0.05$); *$p<0.05$; **$p<0.01$, ***$p<0.001$.

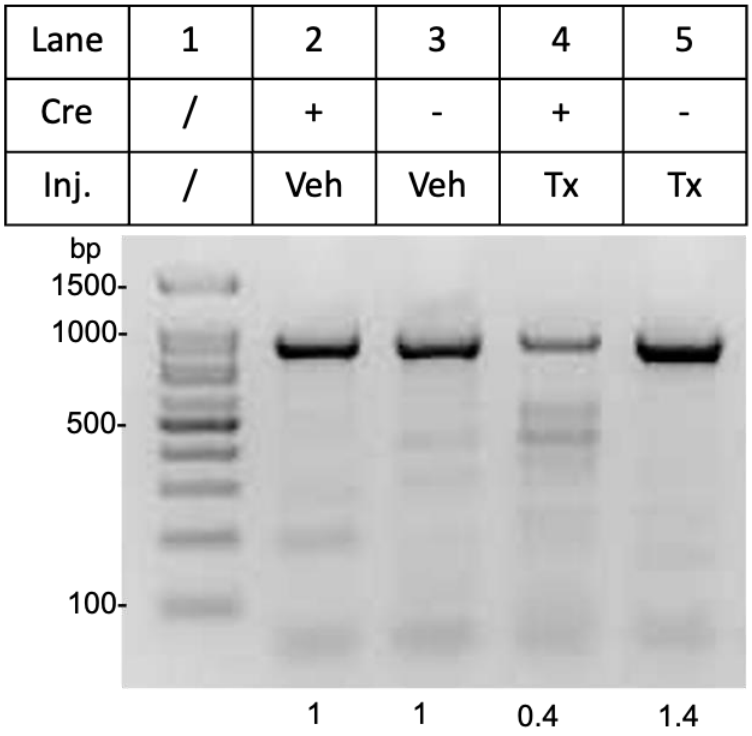

Figure 13: Gel-based analysis of endpoint RT-PCR of *Pdzk1* mRNA from mouse peritoneal macrophages of *Csf1r-iCre Pdzk1*$^{flox/flox}$ *ROSA26*$^{mT/mG}$ mice.

Csf1r-iCre (+) and *Csf1r-iCre* (-) *Pdzk1*$^{flox/flox}$ *ROSA26*$^{mT/mG}$ female mice were injected intra-peritoneally for 5 consecutive days with 166mg of tamoxifen (Tx) per kg of mouse to induce Cre activity, or an equivalent volume of vehicle (Veh; corn oil). Thioglycollate-elicited peritoneal macrophages were harvested one week following the last injection and cultured for 3 days in DMEM and 10% FBS. RNA was collected, reverse transcribed into cDNA and subjected to PCR. cDNA samples were amplified by PCR using primer-pair (PP)2 forward primer with PP4 reverse primer producing a band at 887bp. PCR samples were separated by agarose (1.5%) gel electrophoresis alongside a 1kbp DNA ladder. The gel was visualized and band width and intensity were measured

by ImageJ with values shown at the bottom of each lane (values are relative to lane #2 set to 1).

*PCR and gel electrophoresis were performed by Yak Deng.

4.7.2. Western blotting in peritoneal macrophages from *Csf1r-iCre* *Pdzk1*$^{flox/flox}$ *ROSA26*$^{mT/mG}$ mice

To determine if reductions in *Pdzk1* transcript levels corresponded to reductions in protein, SDS-PAGE/Western blotting was performed (Supplementary Figure 6). Protein extracts of macrophages from tamoxifen-treated or vehicle-treated Cre-positive and Cre-negative mice were assessed by Western blotting using amino- and carboxy-terminal PDZK1 antibodies. GFP and SR-B1 proteins were also examined. There were no apparent changes in the intensity of the 70kDa band (detected by both amino- and carboxy-terminal PDZK1 antibodies) in macrophages from tamoxifen-treated Cre-positive mice compared to controls, despite the presence of GFP protein (indicating active Cre). There was also no apparent change in SR-B1 protein. Therefore, although *Pdzk1* transcripts were significantly reduced using all primer-pairs (Figure 12), the band at 70kDa was not reduced.

4.8.HDL-dependent protection against necroptosis in Cre-mediated *Pdzk1* conditional knockout macrophages

Despite an inability to detect a reduction in PDZK1 protein in Cre-mediated *Pdzk1* conditional knockout macrophages, there was a significant reduction in *Pdzk1* mRNA using all primer-pairs. Therefore, I decided to assess how the Cre-targeted mutation affects HDL-dependent protection of macrophages from necroptosis in the *Pdzk1* conditional knockout macrophages compared to controls. To assess HDL-dependent protection from necroptosis, macrophages from tamoxifen-treated or vehicle-treated Cre-positive mice and tamoxifen-treated Cre-negative mice were treated with TNF-α and z-VAD-FMK in the presence or absence of HDL (Figure 14). In this experiment, cells were stained with SYTOX™ Deep-Red dye which enters and stains the nucleus of cells with compromised plasma membranes (necroptotic cells) but not cells with intact membranes. Moreover, SYTOX™ Deep-Red is a far-red fluorescent dye which was detected using a confocal microscope since that instrument was able to excite SYTOX™ Deep-Red using lasers of specified wavelengths without the excitation of tdTomato. Results showed that TNF-α + z-VAD-FMK induced cell death in vehicle-treated Cre-positive macrophages (~50% of cells were SYTOX™ Deep-Red (+)) compared to untreated and DMSO-treated controls. HDL was able to significantly reduce the level of necroptosis in control macrophages (vehicle-treated Cre-positive and tamoxifen-treated Cre-negative cells, identified by tdTomato fluorescence) compared to the TNF-α + z-VAD-FMK-treated condition, but did not significantly reduce levels of necroptosis in macrophages with a conditional knockout in *Pdzk1* (tamoxifen-treated Cre-positive cells, identified by EGFP

fluorescence) (Figure 14). These results demonstrate that PDZK1 promotes HDL-dependent protection of macrophages from necroptotic cell death.

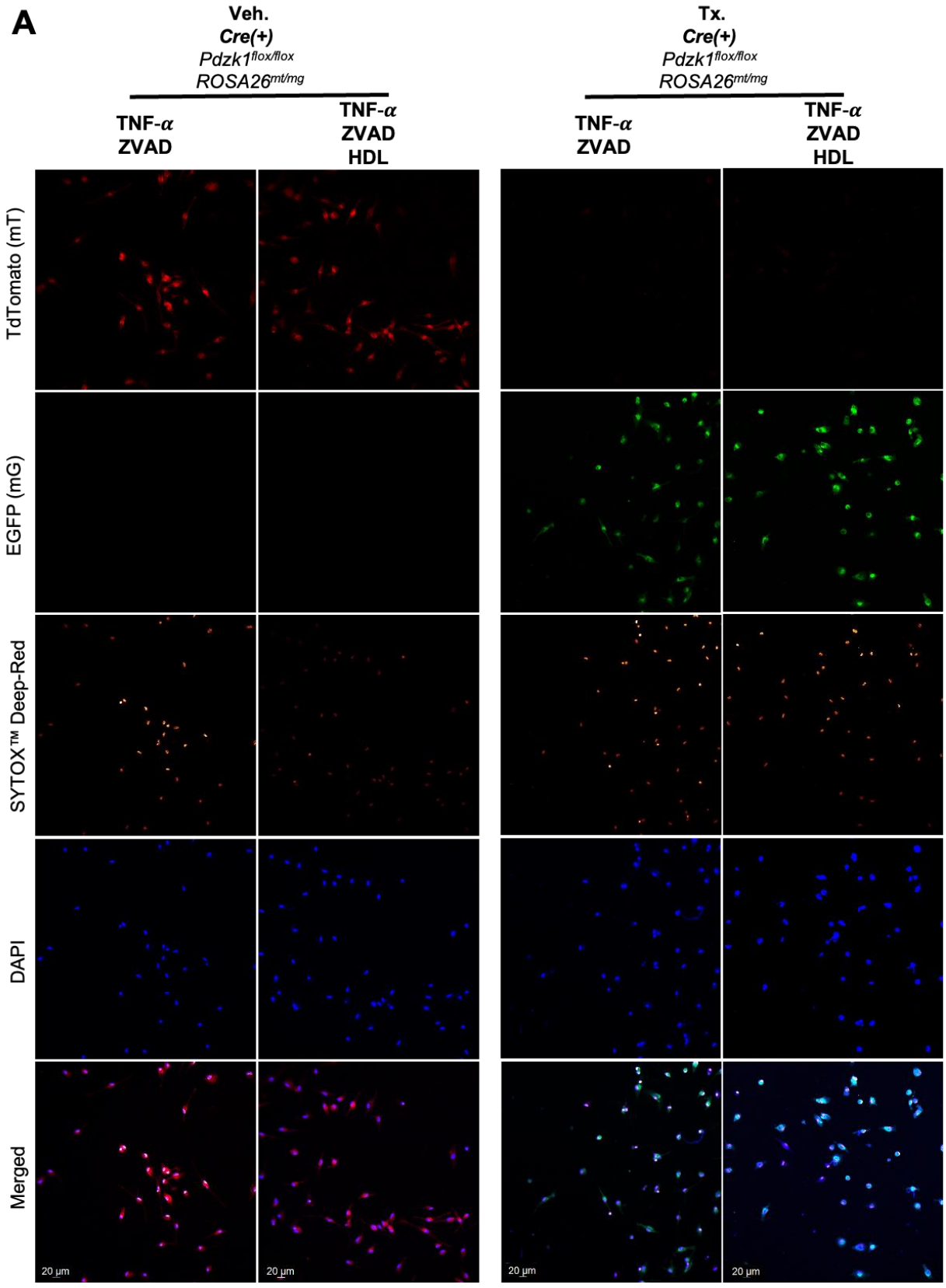
A
Veh.
Cre(+)
Pdzk1flox/flox
ROSA26mt/mg
TNF-α
ZVAD
TNF-α
ZVAD
HDL
Tx.
Cre(+)
Pdzk1flox/flox
ROSA26mt/mg
TNF-α
ZVAD
TNF-α
ZVAD
HDL
TdTomato (mT)
EGFP (mG)
SYTOX™ Deep-Red
DAPI
Merged
20 μm
20 μm
20 μm
20 μm

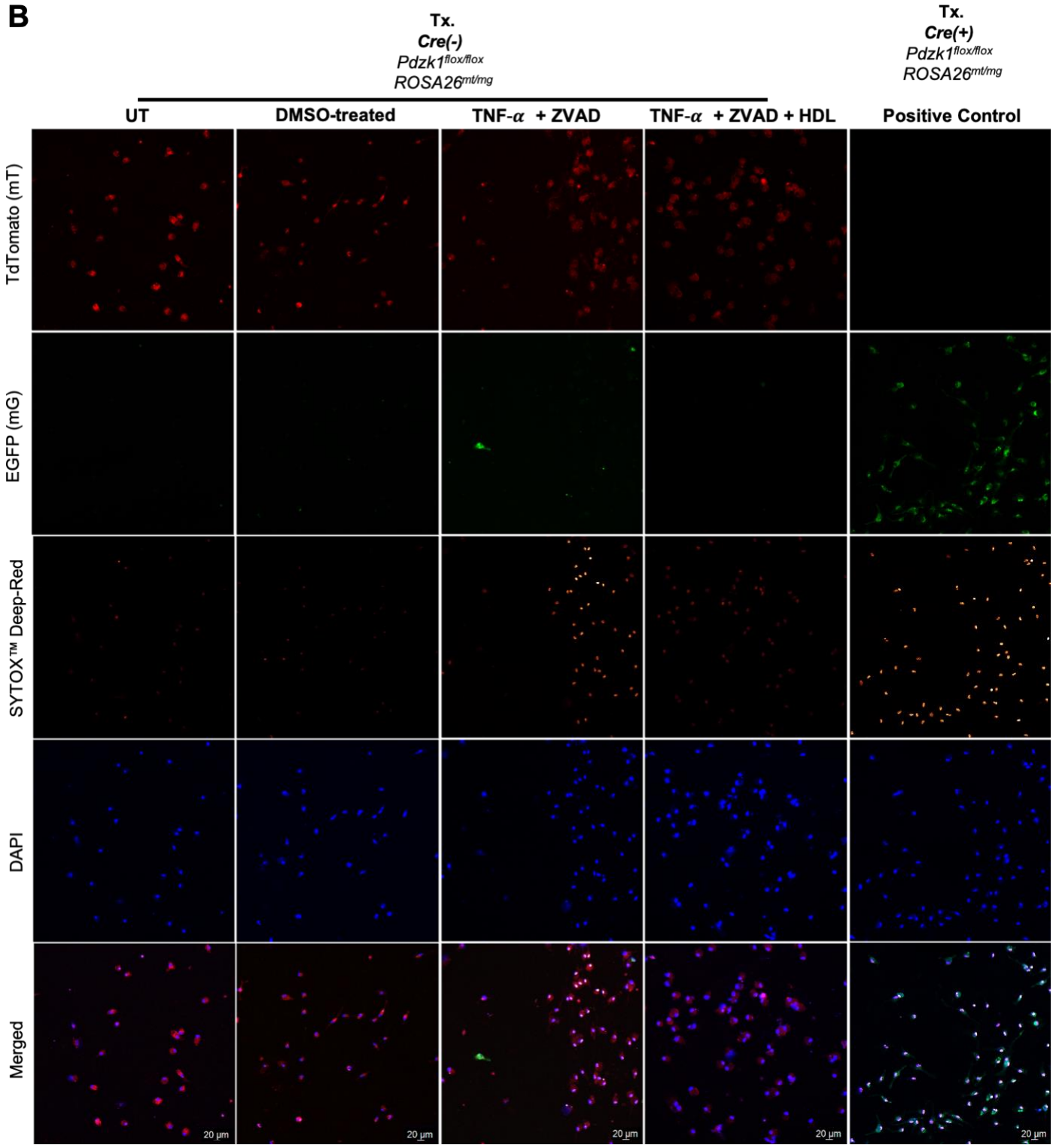
B
Tx.
Cre(-)
Pdzk1flox/flox
ROSA26mt/mg
Tx.
Cre(+)
Pdzk1flox/flox
ROSA26mt/mg
UT
DMSO-treated
TNF-α + ZVAD
TNF-α + ZVAD + HDL
Positive Control
TdTomato (mT)
EGFP (mG)
SYTOX™ Deep-Red
DAPI
Merged
20 μm

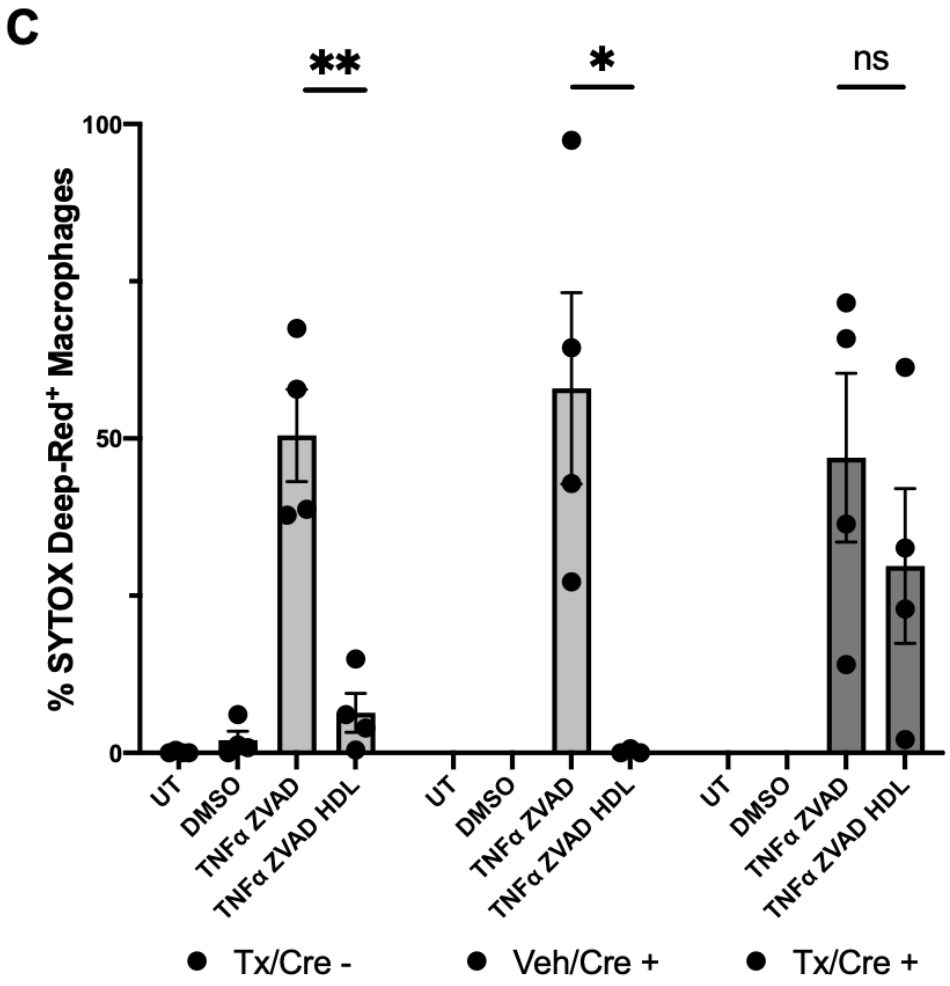

Figure 14: HDL-dependent protection against necroptosis in *Csf1r-iCre Pdzk1$^{flox/flox}$ ROSA26$^{mt/mg}$* mouse peritoneal macrophages.

Csf1r-iCre (+) and *Csf1r-iCre* (-) *Pdzk1$^{flox/flox}$ ROSA26$^{mt/mg}$* male mice were injected intra-peritoneally for 5 consecutive days with 166mg of tamoxifen (Tx) per kg of mouse to induce Cre activity, or an equivalent volume of vehicle (Veh; corn oil). Thioglycollate-elicited peritoneal macrophages were harvested one week following the last injection, cultured in DMEM + 10% FBS for 24h, switched to DMEM + 3% NCLPDS for 24h, then treated. Cells were left untreated (UT) or

incubated with media containing either 0.5% DMSO (v/v), mouse TNF-α (50 ng/mL) and z-VAD-FMK (50μM), or TNF-α, z-VAD-FMK and human HDL (50 μg/mL) for 24 h in DMEM + 3% NCLPDS. Following 24h, cells were stained with SYTOX™ Deep-Red to label the nucleus of necroptotic cells (pseudo yellow/orange color), fixed, then counterstained with DAPI (blue). Cells were imaged using a confocal microscope. (**A**) Representative images (merged image and different channels) of vehicle-treated and tamoxifen-treated Cre-positive macrophages treated with TNF-α + z-VAD-FMK or TNF-α + z-VAD-FMK + HDL. (**B**) Representative images (merged image and different channels) of macrophages from tamoxifen-treated Cre-negative mice that were left untreated or treated with either DMSO, TNF-α + z-VAD-FMK, or TNF-α + z-VAD-FMK + HDL. Positive control (necroptotic) cells were induced by treating with paraformaldehyde before SYTOX™ Deep-Red staining and consisted of macrophages from tamoxifen-treated Cre-positive mice. (**C**) Quantification of the percentage of SYTOX™ Deep-Red (+) cells. DAPI channel is in blue. TdTomato channel is in red. EGFP channel is in green. SYTOX™ Deep-Red channel is in yellow/orange. Data are means ± SEM determined by unpaired student's t-test (N=4 technical replicates per treatment per mouse). NS: not statistically significant ($p>0.05$); *$p<0.05$; **$p<0.01$. Scale bars = 20 µm.

*Treatment of cells and fluorescence imaging were performed by Dr. George Kluck. Mouse injections and analysis were performed by Emmanuel Sakarya.

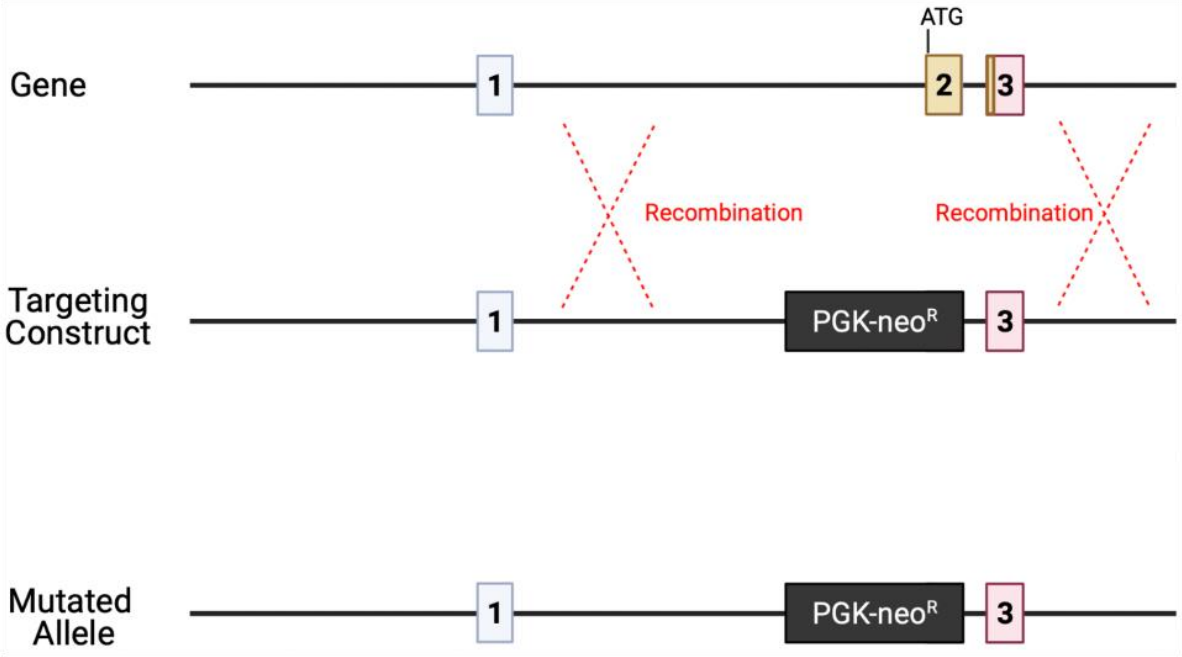

Figure 15: Strategy for generating *Pdzk1-/-* mouse strain.

The upper DNA sequence corresponds to the *Pdzk1* gene from 5' to 3', zoomed into exon 1, 2, and 3 of *Pdzk1*. The middle DNA sequence is the targeting construct consisting of a neomycin resistance cassette (neo^R) driven by the phosphoglycerate kinase (PGK) promoter, that is flanked on both ends by sequences homologous to the sequence to the left and right of exon 2. Homologous recombination of the targeting construct in mouse embryonic stem cells allows for the replacement of exon 2 of *Pdzk1* containing the ATG start codon with PGK-neo^R forming the mutated allele. The rationale for this mutation is that transcription would be confined to PGK-neo^R and absence of an ATG start codon would abolish transcription of a mutated *Pdzk1* mRNA if it were to be transcribed[56].

MASTFNPRECKLSKQEGQNYGFFLRIEKDTDGHLIRVIEEGSPA

EKAGLLDGDRVLRINGVFVDKEEHAQ/VVELVRKSGNSVTLLVLDGDSYEKAV/KNQVDL

KELDQSQREAALNDKKPGPGMNGAVEPCAQPRLCYLVKEGNSFGFSLKTIQGKKGVYL

TNIMPQGVAMKAGVLADDHLIEVNGENVENASHEEVVEKVTKSGSRIMFLLVDKETAR

CHSEQKTQFKRETASLKLLPHQPRVVVIKKGSNGYGFYLRAGPEQKGQIIKDIEPGSP

AEAAGLKNNDLVVAVNGKSVEALDHDGVVEMIRKGGDQTTLLVLDKEAESIYSLARFS

PLLYCQSQELPNGSVKEGPAPIPAPLEATGSEPTEDAEGHKPKLCRLLKEDDSYGFHL

NAIRGQPGSFVKEVQQGGPADKAGLENEDVIIEVNGENVQEEPYDRVVERIKSSGKHV

TLLVCGKMAYSYFQAKKIPIVSSMAEPLVAGPDEKGETSAESEHDAHPAKDRTLSTAS

HSSSNSEDTEM

Figure 16: Mouse PDZK1 amino acid sequence.

Mouse PDZK1 only has one characterized protein isoform of 519 amino acids. The PDZK1 amino acid sequence has been annotated to highlight PDZ domains (PDZ1 in red, PDZ2 in blue, PDZ3 in orange and PDZ4 in purple), carboxylate-binding loops (shaded in yellow), a PKA phosphorylation motif (in green). The sequence to the left of the green-shaded forward slash corresponds to the genomic deletion (exon 2 deletion) in the *Pdzk1-/-* mice which would be missing from the protein. The sequence to the left of the blue-shaded forward slash corresponds to the antigenic sequence used in generating the amino-terminal PDZK1 polyclonal antibody (Abcam, cat: ab121248), however, the antigenic sequence used was the human version of this fragment.

CHAPTER 5: DISCUSSION

Previous studies from our laboratory have shown that *Ldlr* KO mice transplanted with bone marrow stem cells from *Pdzk1* KO mice (*Ldlr* KO$^{BM\text{-}pdzk1KO}$) displayed increased atherosclerosis and necrotic cores compared to *Ldlr* KO mice transplanted with bone marrow stem cells from wild type mice (*Ldlr* KO$^{BM\text{-}WT}$), when fed a high-fat diet [24]. We reasoned that this phenotype might be explained in part by macrophages; one of the more abundant cell types in atherosclerotic plaques. Our laboratory has done extensive studies demonstrating that macrophages from *Pdzk1* KO mice displayed impairments in HDL-dependent protection against cell death (apoptosis and necroptosis) and that this might explain in part the increased necrotic cores observed in plaques from *Pdzk1*/*Ldlr* dKO mice compared to *Ldlr* KO mice (manuscript under review) and in *Ldlr* KO$^{BM\text{-}pdzk1KO}$ mice compared to *Ldlr* KO$^{BM\text{-}WT}$ mice[24]. Indeed, I was able to replicate experiments from our laboratory showing that HDL protects mouse peritoneal macrophages from TNF-α + z-VAD-FMK-induced necroptosis and that this protection was impaired in macrophages from *Pdzk1* KO mice (Figure 4). We believed the explanation for this phenotype was a result of a loss-of-function (null mutation) in *Pdzk1* in macrophages. To sort out what was going on, I did an in-depth investigation of *Pdzk1* expression in macrophages from wild type and *Pdzk1* KO mice. This work also sought to bring clarity on whether or not *Pdzk1* is expressed in macrophages, since others have reported that neither THP-1 macrophages nor mouse peritoneal macrophages express *Pdzk1* because of an inability to detect its mRNA in those cells[47,55]. I was able to detect *Pdzk1* transcript in total RNA extracts from PMA-stimulated THP-1 cells (Figure 2) and

from macrophages from wild type mice (Figure 6-8). Real time qRT-PCR cycle threshold values were in the mid-to-high 20s for macrophages while they were in the low 20s for liver and kidney, indicating that expression levels were higher in kidney and liver compared to macrophages. Additionally, Western blotting in PMA-stimulated THP-1 cells and mouse peritoneal macrophages using a carboxy-terminal PDZK1 antibody (Invitrogen, cat: PA3-16818) provided initial evidence that there is a protein species expressed in these cells at the corresponding molecular weight expected for PDZK1 (~70kDa). The band at 70kDa was induced in PMA-stimulated but not unstimulated THP-1 cells (Supplementary Figure 1) and in peritoneal macrophages cultured in media containing 10% but not 3% serum (Supplementary Figures 2 and 3). However, these changes in protein levels were not explained by changes in *Pdzk1* mRNA expression as detected by real-time qRT-PCR. Therefore, insofar as this band corresponds to PDZK1, the changes observed in protein levels might be explained by changes in PDZK1 protein stabilization and/or mRNA translation. Similar to our findings, PDZK1 protein levels (but not mRNA) has been shown to increase in the livers of Wistar rats following glucagon administration[46]. In addition to total protein, levels of phosphorylated-PDZK1 also increased. This demonstrated that PDZK1 levels are hormonally regulated, and that this regulation might involve cAMP-dependent PKA phosphorylation of PDZK1 on its carboxy-terminal serine residue, since PKA has been shown to phosphorylate PDZK1 at Ser-509 *in vitro* and glucagon is known to increase cellular levels of cAMP and induce PKA activity[46,66]. Nonetheless, it is plausible that increases in serum-derived hormones (such as glucagon or other factors) when switching from media containing 3% to 10%

serum, promotes PDZK1 protein stabilization which might explain results in Supplementary Figures 2 and 3. This can be explored by treating macrophages in media containing 3% serum with different concentrations of glucagon (or other hormones/factors present in calf serum) and then performing Western blotting using anti-PDZK1 antibodies. Phosphorylation status of PDZK1 should also be assessed by Western blotting using anti-phospho PDZK1 antibodies (phospho-PDZK1 antibodies are not commercially available and therefore should be produced in-lab). It is noteworthy that we might not see differences in migration of the 70kDa band due to phosphorylation on a Western blot since this was not observed in the Western blotting from another study despite the presence of phospho-PDZK1[46].

Next, I compared *Pdzk1* mRNA levels in mouse peritoneal macrophages from wild type and *Pdzk1* KO mice (*Pdzk1* KO mice obtained from The Jackson Laboratory; stock No. 006208) to assess the effects of the mutation on *Pdzk1* expression. To our surprise, *Pdzk1* mRNA levels were higher in *Pdzk1-/-* macrophages compared to wild type as assessed by real time qRT-PCR using different *Pdzk1* primer-pairs (PP)2,3,4 and 5, however *Pdzk1* mRNA was absent in the knockout macrophages when using PP1 (Figure 6). This can be reasoned since PP1 hybridizes to exon 2 of *Pdzk1* (Figure 5) which was replaced in the knockout mice with a PGK-neo^R cassette, leaving all other exons intact (Figure 15)[56]. Endpoint RT-PCR and gel electrophoresis was also performed to evaluate the presence of longer transcripts using PP2 forward primer with either PP2,3,4 or 5 reverse primers (Figure 7). Results demonstrated products of the

corresponding sizes in wild type macrophages, while PCR product bands were present and even more intense in *Pdzk1-/-* macrophages consistent with real time qRT-PCR results. Moreover, one of the PCR products in *Pdzk1-/-* macrophages was sequenced and corresponded to a perfect match with a portion of the *Pdzk1* transcript (Figure 8). Altogether, these data suggest that *Pdzk1* is expressed in macrophages (confirming our initial hypothesis), however it is also aberrantly expressed in macrophages from *Pdzk1* KO mice. Macrophages from these "knockouts" may express truncated transcripts missing exon 2 (which codes for a portion of PDZ domain 1 of PDZK1) and it may be possible that such a transcript could be translated into protein because of alternative "atg" start codons found in- or out-of-frame (Figure 5). Additionally, the greater level of transcripts observed in *Pdzk1-/-* macrophages compared to wild type could be explained by the presence of a strong phosphoglycerate kinase (PGK) promoter driving expression of the neomycin resistance gene but which is also adjacent to the remaining exons 3-9 of *Pdzk1*[56]. This is further supported by the fact that heterozygous *Pdzk1+/-* macrophages which have a single PGK-neo^R allele display intermediate levels of *Pdzk1* expression (levels in-between those of wild type and *Pdzk1-/-* macrophages) (Figure 6). Finally, these results are consistent with the literature since it's known that using PGK-neo^R as a selectable marker for gene inactivation can influence expression of neighboring genes[67–71], and it should therefore be removed from the genome after successful insertion by using the Cre-loxP system or another system. A similar situation was reported by Scacheri et. al., in which a targeting mutation in the *Men1* gene, replacing exons 2-4 with PGK-neo^R (inserted in the opposite direction of *Men1* transcription), resulted in abundant expression

of a truncated transcript corresponding to the remaining downstream exons[71]. Although the orientation of the PGK-neo^R cassette in the *Pdzk1-/-* mice I used was not specified by the developers, the PGK promoter can be bi-directional and drive expression of adjacent gene sequences as reported by others[71–73]. However, the precise nature of the transcripts corresponding to *Pdzk1* that were detected in the macrophages from the *Pdzk1* KO mice remains to be fully elucidated.

Seeing that I detected *Pdzk1* mRNA in macrophages from *Pdzk1-/-* mice, liver and kidney of *Pdzk1-/-* mice were also analyzed to see how *Pdzk1* expression compares in these tissues. Compared to wild type, the liver and kidney of *Pdzk1-/-* mice displayed higher levels of *Pdzk1* mRNA using *Pdzk1* PP2 and PP3 but showed no expression with PP1,4, 5 (Figure 9 and 10). Based on the position of these primer-pairs (Figure 5), this data suggests that only the middle portion of the *Pdzk1* transcript (exons 4 and 6, which corresponds to a portion of PDZ domain 2 and 3 of PDZK1) is expressed in these tissues in the *Pdzk1-/-* mice. On the other hand, *Pdzk1-/-* macrophages appear to express transcripts corresponding to exons 4-9 (coding for PDZ domains 2 through 4 and the carboxy-terminus). Finally, Western blotting for PDZK1 in the livers showed absence of the 70kDa band in *Pdzk1-/-* liver compared to wild type liver (Supplementary Figure 5). This makes sense since the carboxy-terminal region of the *Pdzk1* transcript is absent in the liver of *Pdzk1-/-* mice compared to wild type, and therefore it is not being detected by the carboxy-terminal PDZK1 antibody. However, the carboxy-terminal PDZK1 antibody detected a band at 70kDa in macrophages of wild type mice which was also observed in macrophages from *Pdzk1-/-* mice. Although the carboxy-terminal region of the *Pdzk1*

transcript is present in macrophages from *Pdzk1-/-* mice, a deletion of the first 70 amino acids of PDZK1 (~8kDa worth of sequence) is not reflected in the Western blotting results using the carboxy-terminal PDZK1 antibody. There is also no in-frame Methionine (encoded by an in-frame "atg" codon) until amino acid 123 of PDZK1 (Met-123) (Figure 16). Therefore, if PDZK1 was truncated such that it starts from Met-123 then this protein would weigh ~13kDa less than wild type PDZK1 and we would expect that this size difference be reflected by SDS-PAGE/Western blotting using the carboxy-terminal antibody, but it was not. This challenges the reliability of the carboxy-terminal PDZK1 antibody at detecting PDZK1 in macrophages (but not the liver). This suggests that the carboxy-terminal PDZK1 antibody might be cross-reacting with a different protein at 70kDa. This could be addressed by using the carboxy-terminal PDZK1 antibody to immuno-isolate the 70kDa protein species and then sequence it. Lastly, Western blotting results from Supplementary Figure 4 bring into question the reliability of the amino-terminal PDZK1 antibody as it pertains to detecting PDZK1 in macrophages. The amino-terminal antibody (Abcam, cat: ab121248) which was created from amino acids 1-90 of human PDZK1 (Figure 16) is detecting a protein at ~70kDa as well. However, the first 70 amino acids of PDZK1 have been removed by the deletion of exon 2 (confirmed by real time qRT-PCR, see Figure 6) and the remaining amino acids (a.a.71-90) do not have an in-frame Methionine. Therefore, what is this antibody detecting that shows up at 70kDa? The amino-terminal antibody is also detecting a faint band at 70kDa in the liver of *Pdzk1* KO mice, unlike the carboxy-terminal antibody.

Altogether, these data suggest that the amino-terminal and carboxy-terminal antibody might detect a different protein at 70kDa.

Since the macrophages from *Pdzk1* KO mice are not clear-cut null mutants, we would need a true null mutation in *Pdzk1* or considerable reductions in all parts of the *Pdzk1* transcript to study how PDZK1 in macrophages influences HDL-dependent protection against necroptosis. Another method for inactivating *Pdzk1* in macrophages is through the Cre-loxP recombination system using our *Csf1r-iCre Pdzk1*$^{flox/flox}$ *ROSA26*$^{mT/mG}$ mice. In this mouse strain, exon 2 and exon 3 of *Pdzk1* would be removed by Cre, which corresponds to all of PDZ domain 1 and part of PDZ domain 2, respectively (Figure 5). The mouse also has a floxed mT/mG cassette; a fluorescence reporter system making cells fluoresce red initially, but when Cre is expressed and active in macrophages, cells fluoresce green. Our results show that ~85% of cultured peritoneal cells are green-fluorescent, representing macrophages with active Cre (Figure 11). In line with this, we observed reductions in *Pdzk1* transcript in the tamoxifen-treated Cre-positive macrophages of 80%, 50%, 50%, 80%, and 80% for PP1,2,3,4, and 5, respectively (Figure 12). This implies that the remaining 20% of *Pdzk1* transcript (reflected by PP1,4, and 5) might be because of cells that do not have active Cre (as there are around 15% of cells that fluoresce red). The remaining levels of *Pdzk1* transcript could be derived from macrophages not exposed to tamoxifen and/or contaminating, non-macrophage, cells that do not express Cre. It is quite possible that the remaining 15% of red-fluorescent cells are mostly non-macrophage cells, since one study reported that even

after enrichment of thioglycollate-elicited peritoneal macrophages (by adherence to the cell culture dish) there is a residual 12-20% of cells that are non-macrophages[62]. Next, there are a couple of explanations for why PP2 and PP3 do not show the same extent of reduction. The first explanation might be that the real time quantitative PCR amplification is more efficient with these primer-pairs, generating more transcripts. Although the geometric segments of the amplification curves of each primer-pair appear parallel to each other (data not shown), indicating similar efficiencies, primer-pair efficiencies should be assessed quantitatively. A second explanation might be that PP2 and PP3 capture a *Pdzk1* splice-variant that is enriched in the pool of *Pdzk1* mRNA variants. The fold-change in *Pdzk1* expression in macrophages of *Pdzk1-/-* mice relative to WT mice was greater using PP2 and PP3 compared to PP4 and PP5 (Figure 6). Moreover, when comparing levels of *Pdzk1* mRNA in macrophages from WT mice, levels were greater using PP2 and PP3 compared to PP1,4 and 5 (data not shown). This suggests that the exons amplified by PP2 and PP3 (exons 4 and 6; see Figure 5) might contribute to a *Pdzk1* splice variant that is enriched in these tissues.

In addition to real time qRT-PCR, gel-based analysis of endpoint RT-PCR was performed using PP2 forward primer to PP4 reverse primer and showed a reduction of this longer length *Pdzk1* PCR product in tamoxifen-treated Cre-positive macrophages compared to control groups (Figure 13). Altogether, data from real time qRT-PCR and endpoint RT-PCR confirm that the whole *Pdzk1* mRNA transcript is reduced in macrophages. However, Western blotting using both amino- and carboxy-terminal PDZK1 antibodies did not reflect this reduction (Supplementary Figure 6). These results

suggest that the PDZK1 antibodies might be detecting a different protein in macrophages at the corresponding molecular weight of PDZK1. This could be masking the ability to detect changes in PDZK1 protein corresponding to the changes detected in the transcript. This calls into question the reliability and interpretation of the Western blotting results using PDZK1 antibodies in macrophages (Supplementary Figures 1-4 and 6). As suggested earlier, immuno-isolation and sequencing of the 70kDa species should be performed to determine what is detected by the antibody in macrophages.

Since the Cre-mediated *Pdzk1* conditional KO macrophages displayed reductions in *Pdzk1* transcript using all PPs, consistent with what would be expected of a null-mutation, I wanted to take advantage of these cells to test if a null mutation in *Pdzk1* in macrophages impaired HDL-dependent protection against necroptosis. To answer this, I induced necroptosis in mouse peritoneal macrophages from tamoxifen-treated Cre-positive and Cre-negative mice and vehicle-treated Cre-positive mice. Results showed that macrophages from mice that have reduced *Pdzk1* expression (tamoxifen-treated Cre-positive mice) were not protected from necroptosis by HDL, however control macrophages (with wild type *Pdzk1* expression) were protected (Figure 14). This suggests that PDZK1 promotes HDL-dependent protection of macrophages against necroptosis. Despite the presence of truncated *Pdzk1* mRNA species (and possibly truncated protein) in macrophages from *Pdzk1* KO mice, the phenotype of these macrophages (as it pertains to HDL-dependent protection against necroptosis) resembles the phenotype in the Cre-mediated *Pdzk1* conditional knockout.

Up until now, our laboratory's model for HDL-dependent protection of macrophages from cell death consisted of HDL binding to SR-B1 on the extracellular side of the membrane, transmitting a survival signal that required PDZK1 binding to the carboxy-terminal tail of SR-B1 found in the cytoplasm (Figure 17). This connection would culminate in the activation of a pro-survival pathway involving PI3K and AKT (Figure 17). We reasoned this because 1) SR-B1 is a high-affinity receptor for HDL[16] that is expressed in macrophages[74,75]; 2) SR-B1 mediates HDL-dependent signaling in macrophages[29] and other cell types (reviewed in [76]), such as HDL-dependent protection of cardiomyocytes from necrosis[27,28]; 3) PDZK1 is known to bind SR-B1's carboxy-terminal tail via its carboxylate binding loop (CBL) on PDZ domain 1 (high affinity interaction) and PDZ domain 3 (low affinity interaction) (see Figure 16 for CBL sequences)[43,44]; 4) *Pdzk1* gene disruption results in impairment in HDL-dependent migration in endothelial cells[61] and HDL-dependent protection against apoptosis in macrophages[24]. However, both studies from point (4) used the same *Pdzk1* KO mutant mice which we've discovered to express truncated forms of *Pdzk1* in macrophages and therefore the mutation cannot be interpreted as a true null-mutation. In an effort to create a true null mutation, we used the Cre-loxP system for creating a targeting-mutation in *Pdzk1* and we were able to show reductions in all parts of the *Pdzk1* transcript in macrophages. Using this method of *Pdzk1* disruption, our results confirm part of the model from Figure 17; in which PDZK1 promotes HDL-dependent protection of macrophages from necroptosis.

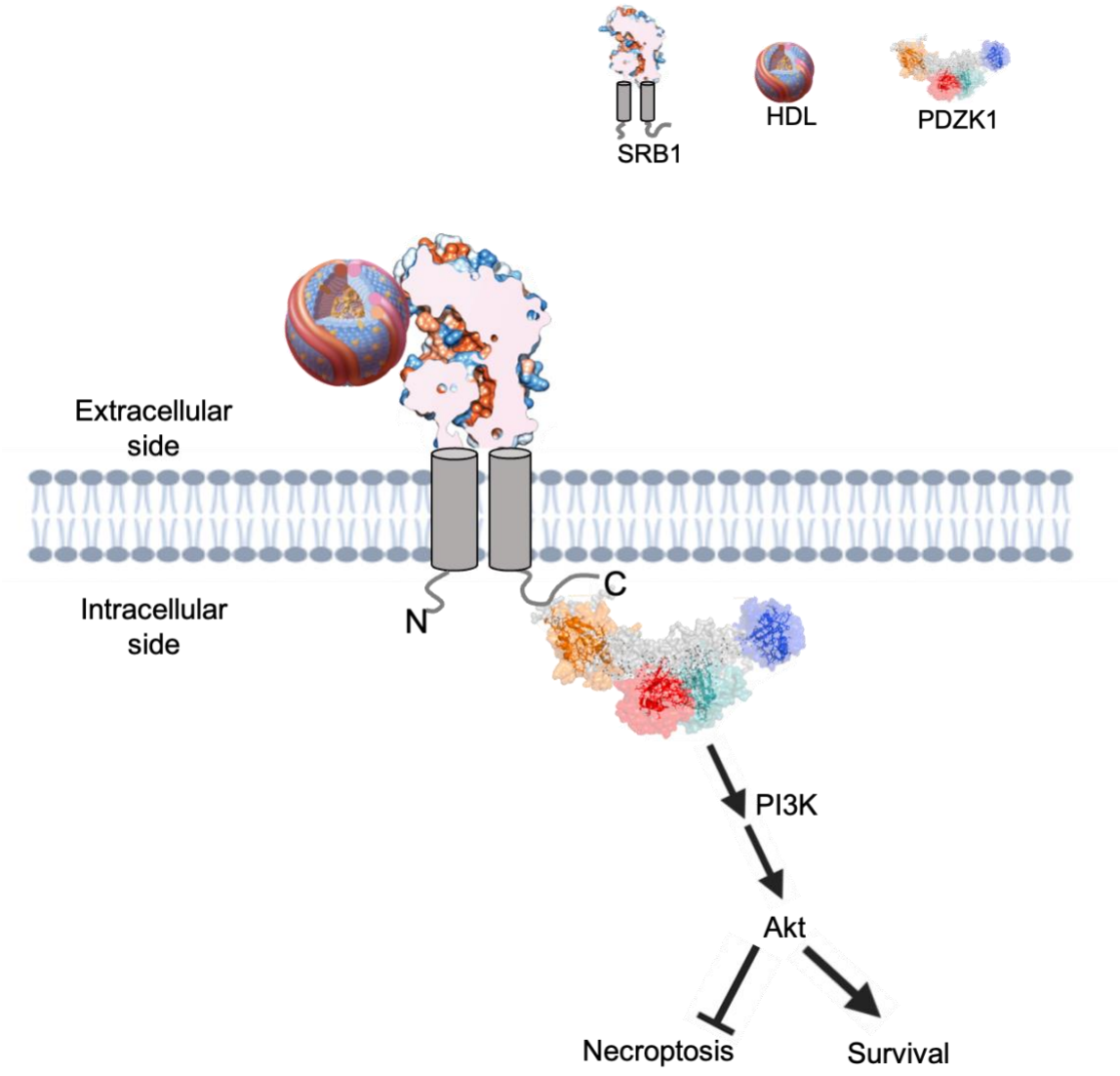

Figure 17: Model of HDL-dependent protection of macrophages from necroptosis.

HDL in the extracellular space binds to SR-B1. PDZK1 binds to SR-B1's carboxy-terminal tail via the carboxylate binding loop in PDZ domain 1. This complex (with or without other proteins) induces an intracellular signaling cascade that involves PI3K and the Akt kinase, promoting survival and inhibiting necroptosis.

*HDL structure (ref. [77]), SR-B1 structure (ref. [78]), PDZK1 structure (ref.[79]).

CONCLUSION

The adaptor protein PDZK1 is commonly known for its athero-protective role in reverse cholesterol transport; by stabilizing SR-B1 protein in the liver, PDZK1 indirectly promotes the elimination of excess cholesterol from peripheral tissues[22]. In addition to this, PDZK1 has recently been involved in athero-protective signaling in key cell types involved in atherosclerosis such as endothelial cells[61], vascular smooth muscle cells[80], and macrophages[24,29]. In this study, we provide insight on the expression of *Pdzk1* in mouse and human macrophages and provide insight on its role in HDL-dependent survival, specifically HDL-dependent protection against necroptotic cell death. This research confirms PDZK1's importance in macrophage biology and should help pave the way for novel research initiatives to understand how PDZK1 in macrophages affects atherosclerosis development as well as how PDZK1's structure relates to its function in macrophages. However, before undertaking such studies, this research highlights the need to identify a reliable and unambiguous method of detecting PDZK1 protein in macrophages. All things considered, these efforts might promote a better understanding of the role of PDZK1 in atherosclerosis and, importantly, allow for more appropriate interpretation of the results using macrophages from *Pdzk1* KO mice.

REFERENCES

1. Wang, H. et al. Global, regional, and national life expectancy, all-cause mortality, and cause-specifi c mortality for 249 causes of death, 1980-2015: a systematic analysis for the Global. *The Lancet* **388**, 1459–1544 (2015).
2. Statistics Canada. Leading causes of death, total population, by age group. https://www150.statcan.gc.ca/t1/tbl1/en/tv.action?pid=1310039401 (2020).
3. Tarride, J.-E. *et al.* A review of the cost of cardiovascular disease. *Can J Cardiol* **25**, 195–201 (2009).
4. Flora, G. D. & Nayak, M. K. A Brief Review of Cardiovascular Diseases, Associated Risk Factors and Current Treatment Regimes. *Current Pharmaceutical Design* **25**, 4063–4084 (2019).
5. Stewart, J., Manmathan, G. & Wilkinson, P. Primary prevention of cardiovascular disease: A review of contemporary guidance and literature. *JRSM Cardiovascular Disease* **6**, 204800401668721 (2017).
6. Linton, M. F. *et al.* The Role of Lipids and Lipoproteins in Atherosclerosis. (2019).
7. Gimbrone, M. A. & García-Cardeña, G. Endothelial Cell Dysfunction and the Pathobiology of Atherosclerosis. *Circulation Research* **118**, 620–636 (2016).
8. Seimon, T. & Tabas, I. Mechanisms and consequences of macrophage apoptosis in atherosclerosis. *Journal of Lipid Research* **50**, (2009).
9. Karunakaran, D. *et al.* Targeting macrophage necroptosis for therapeutic and diagnostic interventions in atherosclerosis. *Science Advances* **2**, (2016).
10. Sun, L. *et al.* Mixed lineage kinase domain-like protein mediates necrosis signaling downstream of RIP3 kinase. *Cell* **148**, 213–227 (2012).
11. Kaczmarek, A., Vandenabeele, P. & Krysko, D. v. Necroptosis: The Release of Damage-Associated Molecular Patterns and Its Physiological Relevance. *Immunity* **38**, 209–223 (2013).
12. Basatemur, G. L., Jørgensen, H. F., Clarke, M. C. H., Bennett, M. R. & Mallat, Z. Vascular smooth muscle cells in atherosclerosis. *Nature Reviews Cardiology* **16**, 727–744 (2019).
13. Gordon, D. J. *et al.* High-density lipoprotein cholesterol and cardiovascular disease. Four prospective American studies. *Circulation* **79**, 8–15 (1989).
14. Krieger, M. Scavenger receptor class b type I is a multiligand hdl receptor that influences diverse physiologic systems. *Journal of Clinical Investigation* **108**, 793–797 (2001).
15. Rothblat, G. H. & Phillips, M. C. High-density lipoprotein heterogeneity and function in reverse cholesterol transport. *Current Opinions in Lipidology* **21**, 229–238 (2010).
16. Acton, S. *et al.* Identificacin of Scavenger Receptor SR-BI as a High Density Lipoprotein Receptor. *Science* **271**, 518–520.
17. Rigotti, A. *et al.* A targeted mutation in the murine gene encoding the high density lipoprotein (HDL) receptor scavenger receptor class B type I reveals its key role in HDL metabolism. *Medical Sciences* **94**, 12610–12615 (1997).

18. Kocher, O. *et al.* Targeted Disruption of the PDZK1 Gene in Mice Causes Tissue-specific Depletion of the High Density Lipoprotein Receptor Scavenger Receptor Class B Type I and Altered Lipoprotein Metabolism. *Journal of Biological Chemistry* **278**, 52820–52825 (2003).
19. Fenske, S. A. *et al.* Normal hepatic cell surface localization of the high density lipoprotein receptor, scavenger receptor class B, type I, depends on all four PDZ domains of PDZK1. *Journal of Biological Chemistry* **284**, 5797–5806 (2009).
20. Braun, A. *et al.* Loss of SR-BI expression leads to the early onset of occlusive atherosclerotic coronary artery disease, spontaneous myocardial infarctions, severe cardiac dysfunction, and premature death in apolipoprotein E-deficient mice. *Circulation Research* **90**, 270–276 (2002).
21. Fuller, M. *et al.* The effects of diet on occlusive coronary artery atherosclerosis and myocardial infarction in scavenger receptor class B, type 1/low-density lipoprotein receptor double knockout mice. *Arteriosclerosis, Thrombosis, and Vascular Biology* **34**, 2394–2403 (2014).
22. Kocher, O. *et al.* Influence of PDZK1 on lipoprotein metabolism and atherosclerosis. *Biochimica et Biophysica Acta - Molecular Basis of Disease* **1782**, 310–316 (2008).
23. Yesilaltay, A., Daniels, K., Pal, R., Krieger, M. & Kocher, O. Loss of PDZK1 causes coronary artery occlusion and myocardial infarction in paigen diet-fed apolipoprotein E deficient mice. *PLoS ONE* **4**, (2009).
24. Yu, P., Qian, A. S., Chathely, K. M. & Trigatti, B. L. PDZK1 in leukocytes protects against cellular apoptosis and necrotic core development in atherosclerotic plaques in high fat diet fed ldl receptor deficient mice. *Atherosclerosis* **276**, 171–181 (2018).
25. Saddar, S., Mineo, C. & Shaul, P. W. Signaling by the high-affinity HDL receptor scavenger receptor B type i. *Arteriosclerosis, Thrombosis, and Vascular Biology* **30**, 144–150 (2010).
26. Yu, P., Qian, A. S., Chathely, K. M. & Trigatti, B. L. Data on leukocyte PDZK1 deficiency affecting macrophage apoptosis but not monocyte recruitment, cell proliferation, macrophage abundance or ER stress in atherosclerotic plaques of LDLR deficient mice. *Data in Brief* **19**, 1148–1161 (2018).
27. Durham, K. K., Chathely, K. M. & Trigatti, B. L. High-density lipoprotein protects cardiomyocytes against necrosis induced by oxygen and glucose deprivation through SR-B1, PI3K, and AKT1 and 2. *Biochemical Journal* **475**, 1253–1265 (2018).
28. Durham, K. K. *et al.* HDL protects against doxorubicin-induced cardiotoxicity in a scavenger receptor class B type 1-, PI3K-, and Akt-dependent manner HDL protects against doxorubicin-induced cardiotoxicity in a scav-enger receptor class B type 1-, PI3K-, and Akt-dependent manner. *Am J Physiol Heart Circ Physiol* **314**, 31–44 (2018).
29. Al-Jarallah, A., Chen, X., González, L. & Trigatti, B. High Density Lipoprotein Stimulated Migration of Macrophages Depends on the Scavenger Receptor Class

B, Type I, PDZK1 and Akt1 and Is Blocked by Sphingosine 1 Phosphate Receptor Antagonists. *PLoS ONE* **9**, (2014).
30. Kocher, O., Comella, N., Tognazzi, K. & Brown, L. F. Identification and partial characterization of PDZK1: a novel protein containing PDZ interaction domains. *Laboratory investigation; a journal of technical methods and pathology* **78**, (1998).
31. Kocher, O. & Krieger, M. Role of the adaptor protein PDZK1 in controlling the HDL receptor SR-BI. *Current Opinion in Lipidology* **20**, 236–241 (2009).
32. Donowitz, M. *et al.* NHERF family and NHE3 regulation. *Journal of Physiology* **567**, 3–11 (2005).
33. Pawson, T. & Scott, J. D. Signaling Through Scaffold, Anchoring, and Adaptor Proteins. *New Series* **278**, 2075–2080 (1997).
34. Lee, H.-J. & Zheng, J. J. PDZ domains and their binding partners: structure, specificity, and modification. *Cell Communication and Signaling* **8**, (2010).
35. Harris, B. Z. & Lim, W. A. Mechanism and role of PDZ domains in signaling complex assembly COMMENTARY Signal Transduction and Cellular Organization. *Journal of Cell Science* **114**, 3219–3231 (2001).
36. Tsunoda, S. *et al.* A multivalent PDZ-domain protein assembles signalling complexes in a G-protein-coupled cascade. *Nature* **388**, 243–249 (1997).
37. Wang, T. & Montell, C. Phototransduction and retinal degeneration in Drosophila. *Pflugers Archiv European Journal of Physiology* **454**, 821–847 (2007).
38. Emi, Y., Nomura, S., Yokota, H. & Sakaguchi, M. ATP-binding cassette transporter isoform C2 localizes to the apical plasma membrane via interactions with scaffolding protein. *Journal of Biochemistry* **149**, 177–189 (2011).
39. Seidler, U. *et al.* The role of the NHERF family of PDZ scaffolding proteins in the regulation of salt and water transport: Lessons learned from knockout mice. *Annals of the New York Academy of Sciences* **1165**, 249–260 (2009).
40. Anzai, N. *et al.* The multivalent PDZ domain-containing protein PDZK1 regulates transport activity of renal urate-anion exchanger URAT1 via its C terminus. *Journal of Biological Chemistry* **279**, 45942–45950 (2004).
41. Lamprecht, G. & Seidler, U. The emerging role of PDZ adapter proteins for regulation of intestinal ion transport. *Am J Physiol Gastrointest Liver Physiol* **291**, 766–777 (2006).
42. Ikemoto, M. *et al.* Identification of a PDZ-domain-containing protein that interacts with the scavenger receptor class B type I. *Proceedings of the National Academy of Sciences* **97**, 6538–6543 (2000).
43. Kocher, O. *et al.* In vitro and in vivo analysis of the binding of the C terminus of the HDL receptor scavenger receptor class B, type I (SR-BI), to the PDZ1 domain of its adaptor protein PDZK1. *Journal of Biological Chemistry* **285**, 34999–35010 (2010).
44. Kocher, O. *et al.* Identification of the PDZ3 domain of the adaptor protein PDZK1 as a second, physiologically functional binding site for the C terminus of the high density lipoprotein receptor scavenger receptor class B type I. *Journal of Biological Chemistry* **286**, 25171–25186 (2011).

45. Tsukamoto, K. *et al.* Noncanonical role of the PDZ4 domain of the adaptor protein PDZK1 in the regulation of the hepatic high density lipoprotein receptor scavenger receptor class B, type i (SR-BI). *Journal of Biological Chemistry* **288**, 19845–19860 (2013).
46. Nakamura, T. *et al.* Regulation of SR-BI protein levels by phosphorylation of its associated protein, PDZK1. *Proceedings of the National Academy of Sciences* **102**, 13404–13409 (2005).
47. Tao, H. *et al.* Macrophage SR-BI mediates efferocytosis via Src/PI3K/Rac1 signaling and reduces atherosclerotic lesion necrosis. *Journal of Lipid Research* **56**, 1449–1460 (2015).
48. Galluzzi, L. *et al.* Molecular mechanisms of cell death: Recommendations of the Nomenclature Committee on Cell Death 2018. *Cell Death and Differentiation* **25**, 486–541 (2018).
49. Tajbakhsh, A. *et al.* Regulation of efferocytosis by caspase-dependent apoptotic cell death in atherosclerosis. *International Journal of Biochemistry and Cell Biology* **120**, (2020).
50. Elliott, M. R., Koster, K. M. & Murphy, P. S. Efferocytosis Signaling in the Regulation of Macrophage Inflammatory Responses. *The Journal of Immunology* **198**, 1387–1394 (2017).
51. Tabas, I. Consequences and therapeutic implications of macrophage apoptosis in atherosclerosis: The importance of lesion stage and phagocytic efficiency. *Arteriosclerosis, Thrombosis, and Vascular Biology* **25**, 2255–2264 (2005).
52. Nofer, J. R. *et al.* Suppression of Endothelial Cell Apoptosis by High Density Lipoproteins (HDL) and HDL-associated Lysosphingolipids. *Journal of Biological Chemistry* **276**, 34480–34485 (2001).
53. Meng, L., Jin, W. & Wang, X. RIP3-mediated necrotic cell death accelerates systematic inflammation and mortality. *Proceedings of the National Academy of Sciences of the United States of America* **112**, 11007–11012 (2015).
54. Lin, J. *et al.* A Role of RIP3-Mediated Macrophage Necrosis in Atherosclerosis Development. *Cell Reports* **3**, 200–210 (2013).
55. Tancevski, I. *et al.* Aspirin regulates expression and function of scavenger receptor-BI in macrophages: studies in primary human macrophages and in mice. *The FASEB Journal* **20**, 1328–1335 (2006).
56. Lan, D. & Silver, D. L. Fenofibrate induces a novel degradation pathway for scavenger receptor B-I independent of PDZK1. *Journal of Biological Chemistry* **280**, 23390–23396 (2005).
57. Huang, L. *et al.* SR-B1 drives endothelial cell LDL transcytosis via DOCK4 to promote atherosclerosis. *Nature* **569**, 565–569 (2019).
58. Zhang, Y. *et al.* Regulation of SR-BI-mediated selective lipid uptake in Chinese hamster ovary-derived cells by protein kinase signaling pathways. *Journal of Lipid Research* **48**, 405–416 (2007).
59. Livak, K. & Piña, A. Analysis of Relative Gene Expression Data Using Real-Time Quantitative PCR and the 2−ΔΔCT Method Related papers Analysis of Relat ive

Gene Expression Dat a Using Real-T ime Quant it at ive PCR and t he 2 C T M…. *methods* **25**, 402–408 (2001).
60. Daigneault, M., Preston, J. A., Marriott, H. M., Whyte, M. K. B. & Dockrell, D. H. The identification of markers of macrophage differentiation in PMA-stimulated THP-1 cells and monocyte-derived macrophages. *PLoS ONE* **5**, (2010).
61. Zhu, W. *et al.* The scavenger receptor class B type I adaptor protein PDZK1 maintains endothelial monolayer integrity. *Circulation Research* **102**, 480–487 (2008).
62. Misharin, A. v., Saber, R. & Perlman, H. Eosinophil contamination of thioglycollate-elicited peritoneal macrophage cultures skews the functional readouts of in vitro assays. *Journal of Leukocyte Biology* **92**, 325–331 (2012).
63. Giral, H. *et al.* Role of PDZK1 protein in apical membrane expression of renal sodium-coupled phosphate transporters. *Journal of Biological Chemistry* **286**, 15032–15042 (2011).
64. Giral, H. *et al.* NHE3 Regulatory Factor 1 (NHERF1) modulates intestinal sodium-dependent phosphate transporter (NaPi-2b) expression in apical microvilli. *Journal of Biological Chemistry* **287**, 35047–35056 (2012).
65. Wang, P. *et al.* Interaction with PDZK1 is required for expression of organic anion transporting protein 1A1 on the hepatocyte surface. *Journal of Biological Chemistry* **280**, 30143–30149 (2005).
66. Janah, L. *et al.* Glucagon receptor signaling and glucagon resistance. *International Journal of Molecular Sciences* **20**, (2019).
67. Zhu, L. *et al.* Craniofacial, skeletal, and cardiac defects associated with altered embryonic murine Zic3 expression following targeted insertion of a PGK-NEO cassette. *Frontiers in Bioscience* **12**, 1680–1690 (2007).
68. Pham, C. T. N., Macivor, D. M., Hug, B. A., Heusel, J. W. & Ley, T. J. Long-range disruption of gene expression by a selectable marker cassette. *Proceedings of the National Academy of Sciences* **93**, 13090–13095 (1996).
69. Li, Z. *et al.* Enhanced expression of human cDNA by phosphoglycerate kinase promoter-puromycin cassette in the mouse transthyretin locus. *Transgenic Research* **20**, 191–200 (2011).
70. Sun, T. & Storb, U. Insertion of Phosphoglycerine Kinase (PGK)-Neo 5 of J 1 Dramatically Enhances VJ 1 Rearrangement. *J. Exp. Med* **193**, 699–711 (2001).
71. Scacheri, P. C. *et al.* Bidirectional Transcriptional Activity of PGK-Neomycin and Unexpected Embryonic Lethality in Heterozygote Chimeric Knockout Mice. *genesis* **30**, 259–263 (2001).
72. Johnson, P. & Friedman, T. Limited bidirectional activity of two housekeeping gene promoters: human HPRT and PGK. *Gene* **88**, 207–213 (1990).
73. Nesterova, T. B. *et al.* Skewing X chromosome choice by modulating sense transcription across the Xist locus. *Genes and Development* **17**, 2177–2190 (2003).
74. Hirano, K.-I. *et al.* Expression of Human Scavenger Receptor Class B Type I in Cultured Human Monocyte-Derived Macrophages and Atherosclerotic Lesions. *Circulation research* **85**, 108–116 (1999).

75. Ji, Y. *et al.* Scavenger receptor BI promotes high density lipoprotein-mediated cellular cholesterol efflux. *Journal of Biological Chemistry* **272**, 20982–20985 (1997).
76. Al-Jarallah, A. & Trigatti, B. L. A role for the scavenger receptor, class B type I in high density lipoprotein dependent activation of cellular signaling pathways. *Biochimica et Biophysica Acta - Molecular and Cell Biology of Lipids* **1801**, 1239–1248 (2010).
77. Huang, R. *et al.* Apolipoprotein A-I structural organization in high-density lipoproteins isolated from human plasma. *Nature Structural and Molecular Biology* **18**, 416–423 (2011).
78. Neculai, D. *et al.* Structure of LIMP-2 provides functional insights with implications for SR-BI and CD36. *Nature* **504**, 172–176 (2013).
79. Hajizadeh, N. R. *et al.* Probing the Architecture of a Multi-PDZ Domain Protein: Structure of PDZK1 in Solution. *Structure* **26**, 1522-1533.e5 (2018).
80. Lee, W. R. *et al.* PDZK1 prevents neointima formation via suppression of breakpoint cluster region kinase in vascular smooth muscle. *PLoS ONE* **10**, (2015).

SUPPLEMENTARY FIGURES

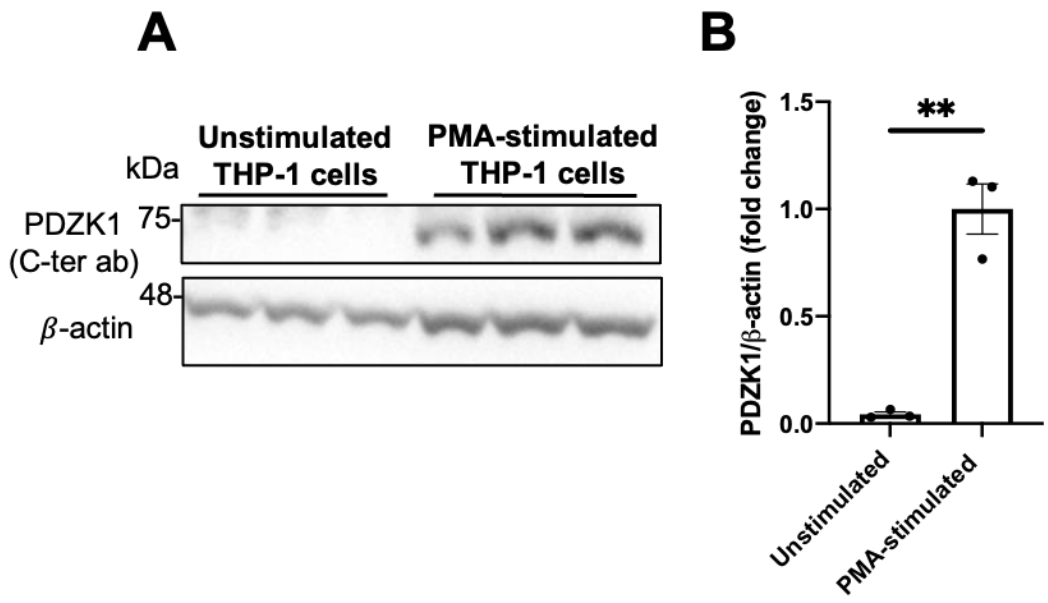

Supplementary Figure 1: Western blotting in unstimulated human THP-1 cells and PMA-stimulated THP-1 cells.

THP-1 monocytes were either left untreated or were differentiated for 48h with 100ng/mL of PMA in RPMI. (**A**) Protein samples were separated by SDS-polyacrylamide (10%) gel electrophoresis, transferred to a PVDF membrane and immunoblotted. Membranes were blocked in 5% milk at room temperature and immunoblotted with anti-PDZK1 (anti-PDZK1 carboxy-terminal antibody; predicted molecular weight of 70kDa) and/or anti-SR-B1 (expected molecular weight of 82kDa). Unstimulated THP-1 cells (N=3 samples) and PMA-stimulated THP-1 cells (N=3 samples) immunoblotted for PDZK1 and β-actin. (**B**) PDZK1/β-actin expression was quantified, and results are shown as means (relative to PMA-stimulated THP-1 cells normalized to 1) ± SEM determined by an unpaired student t-test. **$p<0.01$.

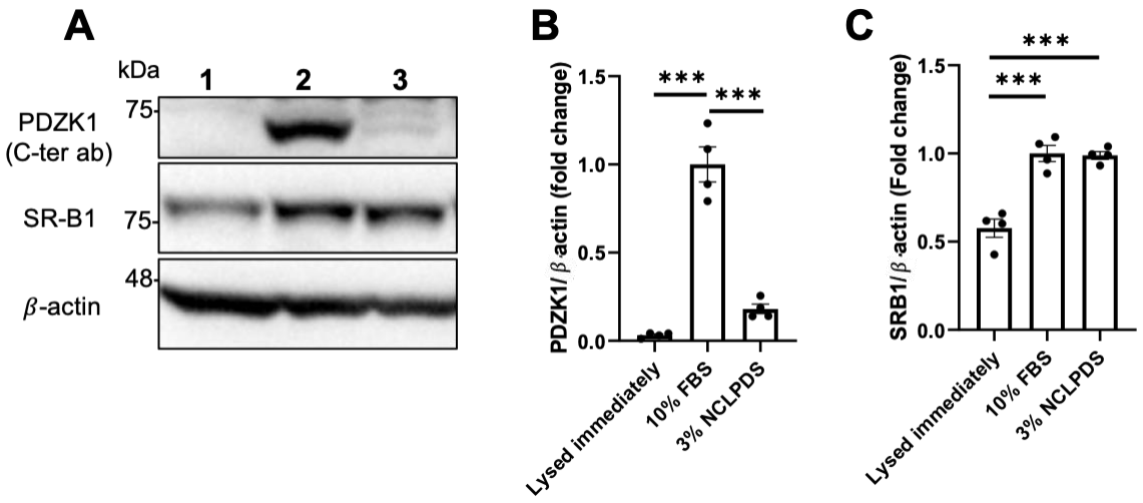

Supplementary Figure 2: Western blotting with antibodies against PDZK1 and SR-B1 in wild type mouse peritoneal macrophages at different time points and varying culture conditions.

Thioglycollate-elicited peritoneal macrophages from WT C57BL/6J male mice (N=4) were either 1) lysed immediately following harvesting (lane 1), 2) cultured in DMEM + 10% FBS for 24h (lane 2), or 3) cultured in DMEM + 10% FBS for 24h then switched to DMEM + 3% NCLPDS for 24h (lane 3). Protein samples were separated by SDS-polyacrylamide (10%) gel electrophoresis, transferred to a PVDF membrane and immunoblotted. Membranes were blocked in 5% milk at room temperature and immunoblotted with anti-PDZK1 antibody (anti-PDZK1 carboxyl-terminal antibody; predicted molecular weight of 70kDa), anti-SR-B1 (expected molecular weight of 82kDa) and anti-β-actin (**A**). PDZK1/β-actin expression (**B**) and SR-B1/β-actin expression (**C**) were quantified, and results are shown as means (relative to condition #2 normalized to 1) ± SEM determined by one-way ANOVA (macrophages from N=4 mice). ***p<0.001.

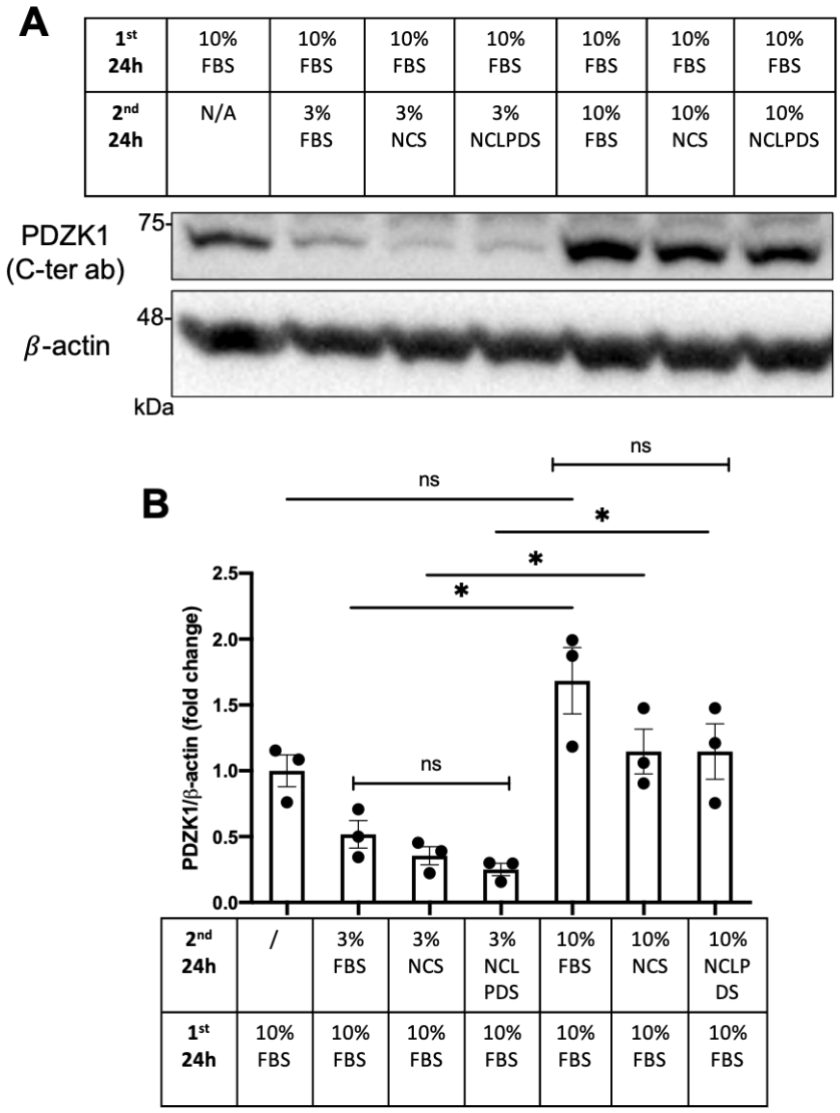

Supplementary Figure 3: Western blotting with an antibody against PDZK1 in wild type mouse peritoneal macrophages under varying time in culture, serum source, serum concentration, and in the presence/absence of lipoproteins.

Thioglycollate-elicited peritoneal macrophages were harvested from WT C57BL/6J male mice (N=3) and cultured in either one of the following 7 conditions. All macrophages were cultured in DMEM and 10% FBS for 24h and were either lysed for

protein collection (lane 1), or cultured for an additional 24h in either DMEM + 3% FBS (lane 2), DMEM + 3% NCS (lane 3), DMEM + 3% NCLPDS (lane 4), DMEM + 10% FBS (lane 5), DMEM + 10% NCS (lane 6), or DMEM + 10% NCLPDS (lane 7). Protein samples were collected following the 2nd 24h incubation and all samples were subjected to SDS-polyacrylamide (10%) gel electrophoresis, transferred onto a PVDF membrane and immunoblotted. Membranes were blocked in 5% milk at room temperature and immunoblotted for PDZK1 (anti-PDZK1 carboxy-terminal antibody; predicted molecular weight of 70kDa) and β-actin (**A**). PDZK1/β-actin expression was quantified (**B**). Results are shown as mean ± SEM determined by unpaired student's t-test (macrophages from N=3 mice) comparing each 3% serum condition with its respective 10% serum condition and comparing 24h DMEM + 10% FBS to 48h DMEM + 10% FBS. NS: not statistically significant ($p>0.05$); *$p<0.05$.

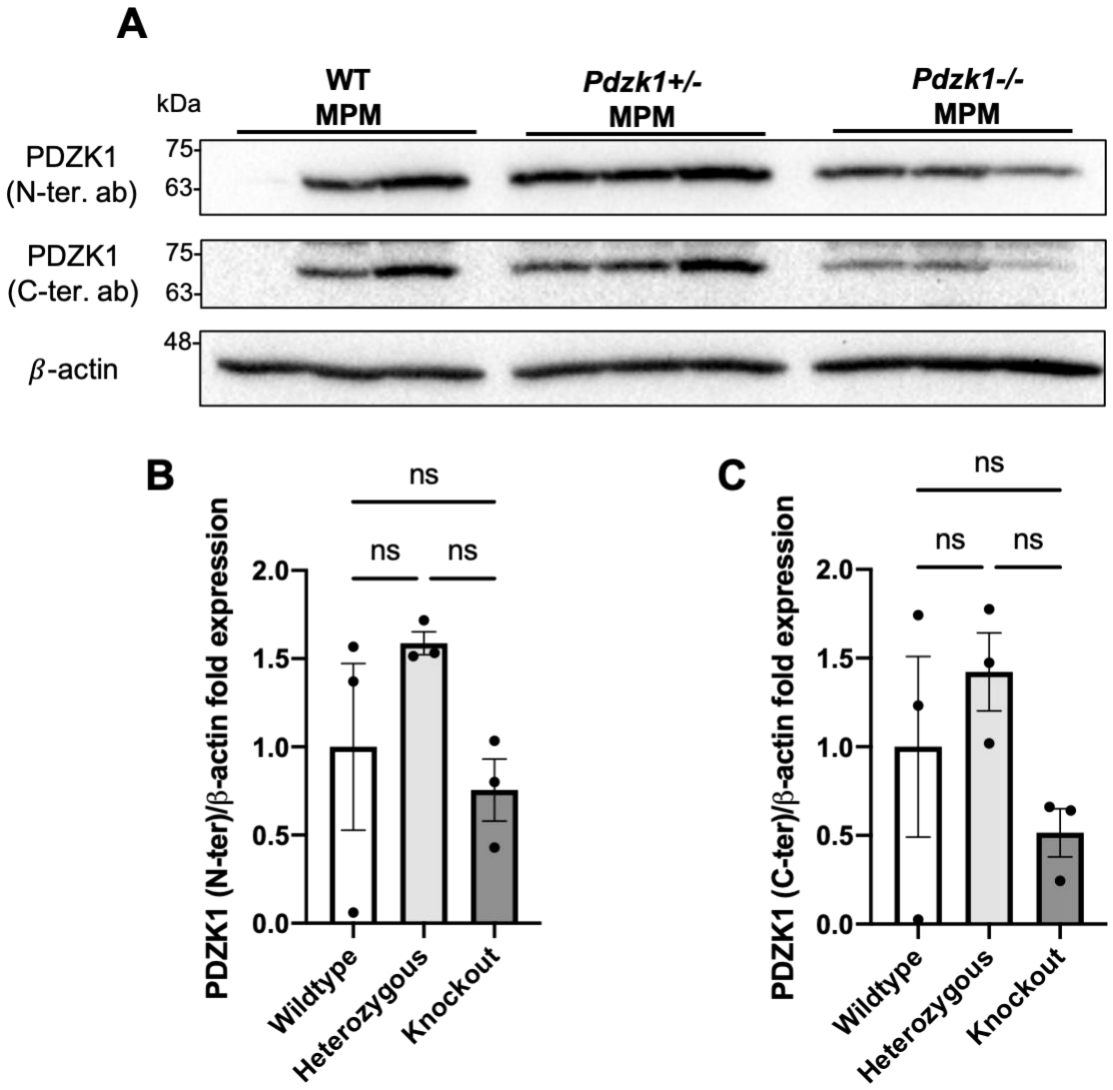

Supplementary Figure 4: Western blotting with antibodies against PDZK1 in WT, *Pdzk1*+/- and *Pdzk1*-/- mouse peritoneal macrophages.

Peritoneal macrophages from WT C57BL/6J, *Pdzk1*+/- and *Pdzk1*-/- male mice were harvested and cultured for 3 days in DMEM and 10% FBS. (**A**) Protein samples were collected and separated by SDS-polyacrylamide (10%) gel electrophoresis, transferred to a PVDF membrane and immunoblotted. Membranes were blocked in 5%

milk at room temperature and immunoblotted for PDZK1 (anti-PDZK1 amino(N)-terminal antibody and anti-PDZK1 carboxy(C)-terminal antibody; both, a predicted molecular weight of 70kDa) and β-actin. PDZK1/β-actin expression was quantified for the N-ter antibody (**B**) and C-ter antibody (**C**) and results are shown as means (relative to WT normalized to 1) ± SEM determined by one-way ANOVA with Tukey's multiple comparisons test (N=3 technical replicates per mouse). NS: not statistically significant ($p>0.05$).

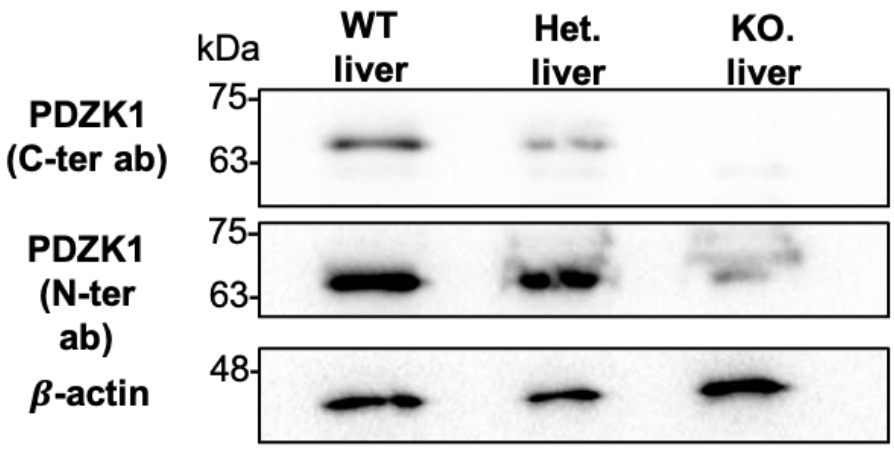

Supplementary Figure 5: Western blotting with antibodies against PDZK1 in WT, *Pdzk1*+/- and *Pdzk1*-/- liver.

Livers from WT C57BL/6J, *Pdzk1*+/- and *Pdzk1*-/- mice were harvested and protein lysates were separated by SDS-polyacrylamide (10%) gel electrophoresis, transferred to a PVDF membrane and immunoblotted. Membranes were blocked in 5% milk at room temperature and immunoblotted using two PDZK1 antibodies (anti-PDZK1 amino-terminal antibody and anti-PDZK1 carboxy-terminal antibody; both, a predicted molecular weight of 70kDa) and β-actin.

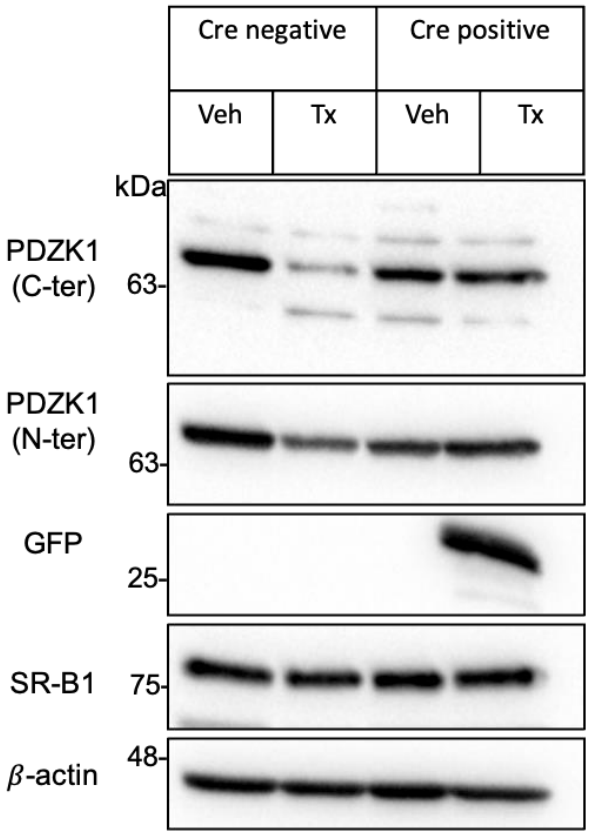

Supplementary Figure 6: Western blotting with antibodies against PDZK1 in peritoneal macrophages from *Csf1r-iCre Pdzk1$^{flox/flox}$ ROSA26$^{mT/mG}$* mice.

Csf1r-iCre (+) and *Csf1r-iCre* (-) *Pdzk1$^{flox/flox}$ ROSA26$^{mT/mG}$* male mice were injected intra-peritoneally for 5 consecutive days with 166mg of tamoxifen (Tx) per kg of mouse to induce Cre activity, or an equivalent volume of vehicle (Veh; corn oil). Thioglycollate-elicited peritoneal macrophages were harvested one week following the last injection and cultured for 3 days in DMEM and 10% FBS. Protein samples were collected and separated by SDS-polyacrylamide (10%) gel electrophoresis, transferred to a PVDF membrane and immunoblotted. Membranes were blocked in 5% milk at room temperature and immunoblotted for PDZK1 (anti-PDZK1 amino-terminal antibody and

anti-PDZK1 carboxy-terminal antibody; both, a predicted molecular weight of 70kDa), GFP (expected molecular weight of 28kDa), SR-B1 (expected molecular weight of 82kDa) and β-actin.